JIPB Journal of Integrative Plant Biology

Research Article
https://doi.org/10.1111/jipb.13326

Abscisic acid-dependent *PMT1* expression regulates salt tolerance by alleviating abscisic acid-mediated reactive oxygen species production in *Arabidopsis*

Qi Yu He[1], Jian Feng Jin[1], He Qiang Lou[2], Feng Feng Dang[3], Ji Ming Xu[1], Shao Jian Zheng[1] and Jian Li Yang[1]*

1. State Key Laboratory of Plant Physiology and Biochemistry, College of Life Sciences, Zhejiang University, Hangzhou 310058, China
2. State Key Laboratory of Subtropical Silviculture, Zhejiang A & F University, Hangzhou 311300, China
3. State Key Laboratory for Conservation and Utilization of Subtropical Agro-Bioresources, South China Agricultural University, Guangzhou 510642, China

*Correspondence: Jian Li Yang (yangjianli@zju.edu.cn)

Qi Yu He

Jian Li Yang

ABSTRACT

Phosphocholine (PCho) is an intermediate metabolite of nonplastid plant membranes that is essential for salt tolerance. However, how PCho metabolism modulates response to salt stress remains unknown. Here, we characterize the role of phosphoethanolamine *N*-methyltransferase 1 (PMT1) in salt stress tolerance in *Arabidopsis thaliana* using a T-DNA insertional mutant, gene-editing alleles, and complemented lines. The *pmt1* mutants showed a severe inhibition of root elongation when exposed to salt stress, but exogenous ChoCl or lecithin rescued this defect. *pmt1* also displayed altered glycerolipid metabolism under salt stress, suggesting that glycerolipids contribute to salt tolerance. Moreover, *pmt1* mutants exhibited altered reactive oxygen species (ROS) accumulation and distribution, reduced cell division activity, and disturbed auxin distribution in the primary root compared with wild-type seedlings. We show that *PMT1* expression is induced by salt stress and relies on the abscisic acid (ABA) signaling pathway, as this induction was abolished in the *aba2-1* and *pyl112458* mutants. However, ABA aggravated the salt sensitivity of the *pmt1* mutants by perturbing ROS distribution in the root tip. Taken together, we propose that PMT1 is an important phosphoethanolamine *N*-methyltransferase participating in root development of primary root elongation under salt stress conditions by balancing ROS production and distribution through ABA signaling.

Keywords: abscisic acid (ABA), oxidative stress, plasma membrane, phosphoethanolamine *N*-methyltransferase, phospholipid metabolism, salt stress

He, Q. Y., Jin, J. F., Lou, H. Q., Dang, F. F., Xu, J. M., Zheng, S. J., and Yang, J. L. (2022). Abscisic acid-dependent *PMT1* expression regulates salt tolerance by alleviating abscisic acid-mediated reactive oxygen species production in *Arabidopsis*. J. Integr. Plant Biol. **64:** 1803–1820.

INTRODUCTION

Salt stress is one of the major environmental stresses for plants and imposes ionic stress, osmotic stress, and a series of secondary effects such as oxidative stress (Yang and Guo, 2018), inducing changes at the molecular, physiological, metabolic, and morphological levels to increase plant survival. With current irrigation practices and climate change, soil salinization is a rising concern that affects over 800 million hectares of land worldwide (Munns and Tester, 2008), therefore threatening global food security. To mitigate this problem, a greater understanding of how plants respond to high salinity is needed (Zhao et al., 2020).

Previous studies have identified many genes encoding proteins engaged in regulatory pathways that coordinate plant responses to salt stress. For instance, the SALT OVERLY SENSITIVE (SOS) signaling pathway is specifically involved in the extrusion of sodium (Na^+) out of cells

(Yang et al., 2019), whereas the mitogen-activated protein kinase (MAPK) cascade participates in salt stress signaling responses in arabidopsis (*Arabidopsis thaliana*) (Yang and Guo, 2018). Osmotic stress activates kinases from the Sucrose non-fermenting 1 (SNF1)-related kinase (SnRK2) family in both an abscisic acid (ABA)-dependent and ABA-independent manner to induce the expression of responsive genes for plant adaptation to stress (Zhao et al., 2018b). In addition to these salt stress responses pathways, the proper functioning of cell organelles plays an essential role in salt tolerance. For example, cell wall integrity influences plant growth and salt stress tolerance (Feng et al., 2018; Zhao et al., 2018a). Similarly, salt-tolerant plants have been reported to maintain the integrity of their plasma membrane (PM) when subjected to salt stress, possibly through the regulation of the lipid and protein composition of their membranes (Mansour, 1995; Salama et al., 2007).

The PM mainly consists of a bilayer of lipid molecules and forms a physical barrier that isolates the cytoplasm from the outside environment. In addition to phosphatidylethanolamine (PE), phosphatidylcholine (PC) is another major phospholipid in non-plastid plant membranes (Bolognese and McGraw, 2000). The main PC biosynthetic pathway in plants is the cytidine diphosphate (CDP)–choline pathway, also referred to as the Kennedy pathway (Kennedy and Weiss, 1956; Jost et al., 2009; Chen et al., 2019). Briefly, PC is synthesized by incorporating the polar head group of phosphocholine (PCho) into the diacylglycerol (DAG) backbone (Cruz-Ramiérez et al., 2004). PCho is an essential precursor for PC whose biosynthesis mainly depends on the *N*-methylation of phosphoethanolamine (PEA), which is catalyzed by phosphoethanolamine *N*-methyltransferases (PMTs) in plants. The Arabidopsis genome has three *PMT* genes (Chen et al., 2018, 2019): *PMT1* (At3g18000), *PMT2* (At1g48600), and *PMT3* (At1g73600). Previous studies have shown that PMT1 plays a critical role in phospholipid metabolism, and loss of PMT1 function impairs root development and epidermal cell integrity of seedlings grown on half-strength Murashige and Skoog (½MS) growth medium (Cruz-Ramiérez et al., 2004; Chen et al., 2019). However, Mou et al. (2002) presented contradictory results, whereby the partial silencing of *PMT1* via expression of an antisense RNA had no effects on root growth on ½MS growth medium, but showed hypersensitivity to salt stress (Mou et al., 2002). These results suggest that phospholipid metabolism is involved in salt stress, but its underlying mechanism needs further investigation.

The phytohormone ABA not only affects plant growth and development but also participates in plant responses to various abiotic stresses such as drought and high salinity (Yoshida et al., 2019; Kamiyama et al., 2021). ABA contents rise under osmotic stress conditions via increased biosynthesis and reduced catabolism (Zhu, 2002; Barrero et al., 2006), which triggers ABA-dependent downstream responses. Notably, ABA exerts dual roles in root growth. First, low concentrations of exogenously applied ABA promote root growth, which is mainly achieved by inhibiting cell division in the quiescent center (QC) and suppressing the differentiation of stem cells and their daughters in the Arabidopsis root meristem (Zhang et al., 2010). Second, high concentrations of ABA inhibit root elongation by inducing the production of reactive oxygen species (ROS), as evidenced in a mutant in *ABA OVERLY SENSITIVE8* (*ABO8*) (Yang et al., 2014). The sensitivity of primary root growth to ABA treatment in *arf2* (*auxin response factor 2*) mutants showed that ABA signals crosstalk with auxin signals to maintain normal root growth (Wang et al., 2011). In addition, the ABA signaling pathway can also alter root development by regulating DNA replication and ethylene signaling (Sun et al., 2018). Therefore, understanding the mechanisms by which ABA regulates root development by interacting with other factors, such as PCho biosynthesis, may offer clues to improve growth and development of plants under salt stress conditions.

In this present study, we identified the T-DNA insertion mutant SALK_108751 with a hypersensitive phenotype to salt and osmotic stress. We demonstrate here that this phenotype is caused by the loss of PMT1 function, a PMT. Compared with wild-type (WT) plants, *pmt1* mutants displayed severe loss of cell membrane integrity and cell division activity as well as a disrupted ROS distribution pattern along the root apex. These phenotypes were not associated with an imbalance of the potassium K^+/Na^+ ratio but with altered glycerolipid metabolism under salt stress. The expression of *PMT1* was induced by salt stress, which was dependent on salt-induced ABA signaling. Notably, ABA accumulated in the *pmt1* mutants in response to the altered ROS production and distribution under salt stress in the mutants, resulting in salt toxicity. Taken together, we conclude that, while salt stress-induced ABA accumulation is involved in the induction of *PMT1* expression, ABA also contributes to ROS production, which leads to salt toxicity. We propose a novel regulatory layer whereby PMT1-mediated glycerolipid metabolism protects the root apex from salt toxicity by alleviating ABA-induced ROS production in *Arabidopsis*.

RESULTS

Identification of a T-DNA insertion mutant hypersensitive to salt stress

To identify genes required for salt tolerance, we collected Arabidopsis T-DNA insertion mutants and tested their primary root elongation when grown on growth medium containing 80 mM NaCl. We noticed one T-DNA mutant line (SALK_108751) with severe inhibition of root elongation under these conditions (Figure 1A, B). However, shoot growth of SALK_108751 appeared to be normal even when experiencing NaCl stress (Figure 1A). Seedlings of SALK_108751 also produced more lateral roots than WT seedlings under NaCl stress (Figure 1C). To distinguish between ion toxicity and osmotic stress as the possible cause of the inhibition of root elongation seen in the mutant, we exposed seedlings to 200 mM mannitol or 25% polyethylene glycol (PEG). Root

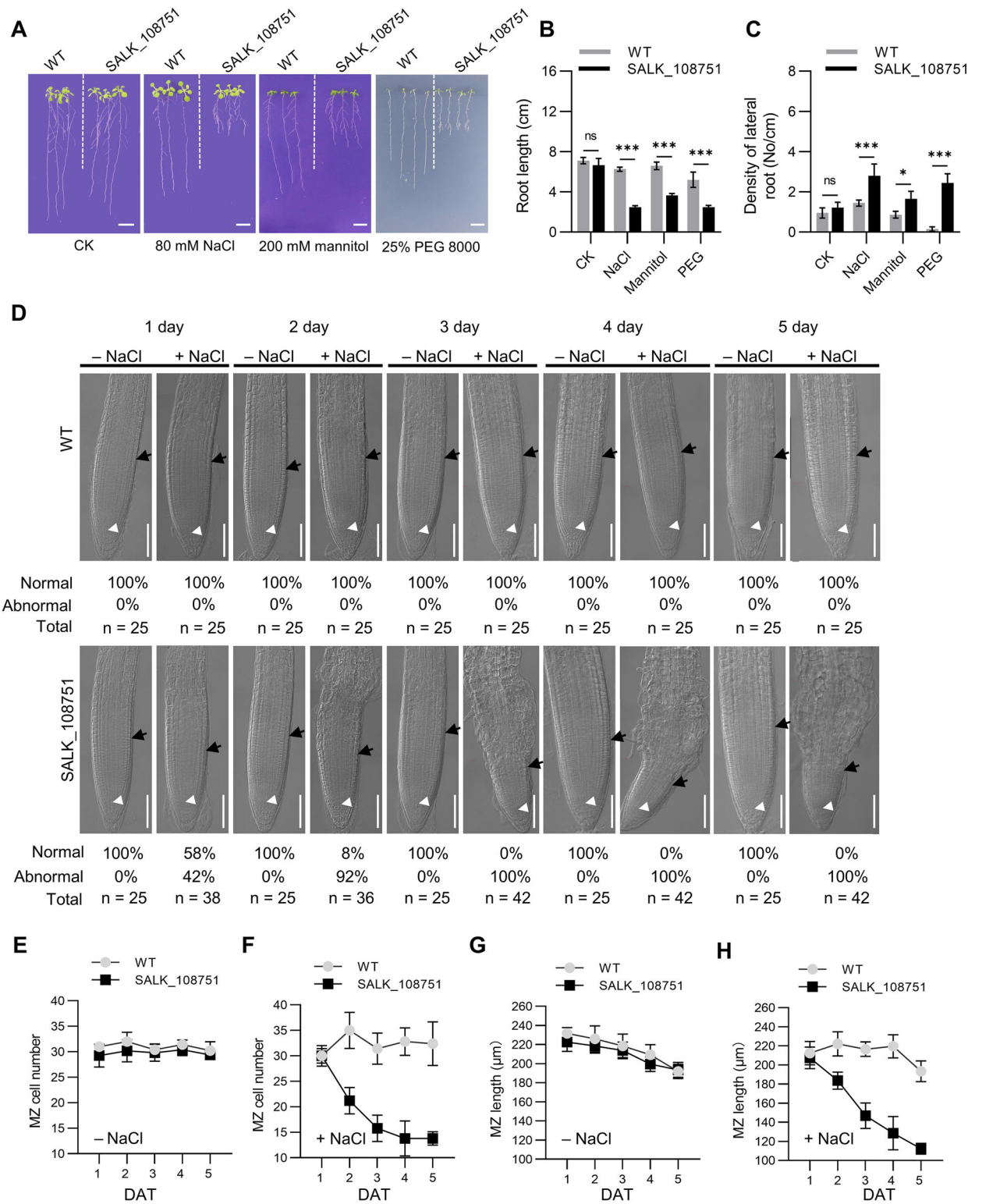

Figure 1. A T-DNA insertion mutant SALK_108751 showed hypersensitivity to high concentrations of salts

(A) Phenotype analysis of SALK_108751 upon salt, mannitol and polyethylene glycol (PEG) treatment. Here, 5-d-old seedlings of wild-type (WT) and SALK_108751 were transferred to 1/5 Hoagland growth medium without (CK) or with 80 mM NaCl, 200 mM mannitol, and 25% PEG for 7 d. Bars = 1 cm. **(B)** Root length, and **(C)** Lateral root density in **(A)** were calculated. Values are means ± *SD* ($n \geq 3$). **(D)** Differential interference contrast (DIC) microscopy images showing primary root of WT and SALK_108751 in 1/5 Hoagland growth medium with or without 80 mM NaCl over 5 d. Bars = 100 μm. The percentages of normal and abnormal primary root were calculated. Black arrows indicate the position of the boundary of meristem zone (MZ), and white arrows indicate the position of the quiescent center (QC). **(E–H)** Quantification of MZ cell number **(E, F)** and MZ length **(G, H)** of 5-d-old seedlings of WT and SALK_108751 without **(E, G)** or with **(F, H)** NaCl treatment for 1-5 d after transferring (DAT). Values are means ± *SD*. Statistical analysis was performed using Student's *t*-test (ns, not significant; $^*P < 0.05$; $^{***}P < 0.001$).

elongation of SALK_108751 was also hypersensitive to osmotic stress (Figure 1A–C).

To further characterize the salt-sensitive phenotype of the SALK_108751 line, we investigated the morphological changes at the root apex under NaCl stress using differential interference contrast (DIC) microscopy. We observed no obvious morphological changes in the root apex of WT seedlings over 5 d of NaCl treatment (Figure 1D). However, approximately 42% ($n = 38$) of all root apices from SALK_108751 seedlings began to exhibit an aberrant morphology during the first day of salt stress, although the number of cells in the meristem zone (MZ) and MZ length in the mutant were comparable with those of WT seedlings (Figure 1E–H). Importantly, most (93%, $n = 36$) root apices displayed an abnormal appearance by the second day of salt stress, which coincided with a significant reduction in MZ cell number and MZ length (Figure 1E–H). The effect on MZ cell number and MZ length was exacerbated by longer exposure to salt stress and was accompanied by premature protoxylem differentiation (Figure S1A–C). Moreover, we noticed that root hairs and lateral roots form closer to the QC in the mutant relative to WT seedlings (Figure S1D).

To examine the specificity of SALK_108751 to various salt species, we compared the root growth response of SALK_108751 and the WT to other salts. Surprisingly, SALK_108751 also displayed severe inhibition of root growth in response to 60 mM $NaNO_3$ (Figure S2B, C), 80 mM KCl (Figure S2D, F), 40 mM $CaCl_2$ (Figure S2G, I), and 20 mM Na_2SO_4 (Figure S2H, I). Salt stress is generally associated with a disturbance of Na^+/K^+ homeostasis. However, SALK_108751 also showed hypersensitivity to 40 mM NaCl and 40 mM KCl (Figure S2E, F). We conclude that SALK_108751 is an interesting mutant exhibiting broad-spectrum sensitivity to high salt concentrations.

PMT1 is responsible for root growth under salt stress

Based on information from the Arabidopsis Biological Resource Center (ABRC), SALK_108751 harbored three T-DNA insertions (Figure S3A). The first insertion resides in the intergenic region between At1g47770 and At1g47780 but had no effect on the transcript levels of either gene (Figure S3B). The second insertion is in the third intron of At5g14780, resulting in lower transcript levels for *FORMATE DEHYDROGENASE* (*FDH*) (Figure S3C). These results indicated that SALK_108751 is a knockdown mutant for *FDH*. To test whether this *FDH* knockdown allele is responsible for the salt-sensitive phenotype of SALK_108751, we obtained another two T-DNA insertion mutant lines (*fdh1-1*, SALK_117670; *fdh1-2*, SALK_088182) from the ABRC. The *fdh1-1* and *fdh1-2* mutants carry a T-DNA insertion in the first intron and 5′ untranslated region (5′ UTR) of the gene, respectively. RT-PCR analysis indicated that *fdh1-1* is a knockout (*ko*) allele, whereas *fdh1-2* is an overexpressing line of *FDH* (Figure S3C). However, we observed no difference between either mutant and WT seedlings under the same conditions that produced a phenotype with SALK_108751, indicating that *FDH* is unlikely to be the causal gene (Figure S3D, E). The third insertion is in the eighth exon of At3g18000 (*PMT1*), and this insertion influenced its transcript levels (Figure S3B). *PMT1* encodes PMT, which is required for phosphocholine (PCho) biosynthesis (Alatorre-Cobos et al., 2012; Liu et al., 2018, 2019). Mutants in *PMT1* exhibit defects in primary root elongation, which can be rescued by an exogenous supply of Cho. Importantly, the addition of 100 μM ChoCl to the growth medium fully rescued the sensitivity of SALK_108751 to NaCl stress (Figure S4), suggesting that the loss of PMT1 function is responsible for the salt-sensitive phenotype of SALK_108751.

To validate the contribution of PMT1 to salt tolerance, we generated additional *pmt1* mutants by clustered regularly interspaced short palindromic repeats (CRISPR)/CRISPR-associated nuclease 9 (Cas9)-mediated gene editing (Xing et al., 2014) with two pairs of single guide RNAs (sgRNA) (Figure 2A). We identified three homozygous mutants, namely *pmt1-1*, *pmt1-2*, and *pmt1-3*. The *pmt1-1* mutant harbored a 194-bp deletion between the sixth exon and sixth intron; *pmt1-2* had a 101-bp deletion in the eighth exon, and *pmt1-3* carried a 1-bp insertion and a 2-bp deletion (Figure 2A). All three gene-edited mutants showed severe root growth defects under NaCl stress conditions (Figure 2B, D). We also generated complementation lines by introducing the full genomic sequence of *PMT1* cloned in-frame with the sequence of the green fluorescent protein (*GFP*) driven by the *PMT1* promoter (*ProPMT1:PMT1-GFP*) into SALK_108751. We obtained two independent complementation lines (*Comp #1* and *Comp #2*) that showed a full rescue of the hypersensitivity phenotype to salt stress relative to WT seedlings, suggesting that the mutation of *PMT1* is responsible for the observed salt sensitivity seen in SALK_108751 (Figure 2C, E). We also isolated two lines overexpressing *PMT1* (OE5 and OE6), with an over two-fold increase in *PMT1* transcript levels (Figure S5). Whereas we measured no difference in root growth under control conditions in these lines (Figure 2F, G), they displayed greater root growth than WT seedlings under salt stress conditions (Figure 2H, I).

PMT1, but not its paralogs, plays a major role in regulating salt tolerance

The *Arabidopsis* genome encodes three PMT proteins. To explore potential redundancy between members of the *PMT* family, we isolated *pmt2* and *pmt3* loss-of-function mutants via CRISPR/Cas9 gene editing (Figure S6A–D). The *pmt2* and *pmt3* single mutants showed no obvious phenotype when subjected to NaCl treatment (Figure S6E, F). We also attempted to obtain *pmt1-2 pmt2* and *pmt2 pmt3* double mutants but failed to harvest seeds from *pmt1-2 pmt3* double mutant plants because of severe defects in development (Figure S7C). However, we obtained *pmt1-2 pmt2* and *pmt2 pmt3* double mutants, whose seedling roots were shorter than those of WT seedlings under normal conditions. Upon salt treatment, the root length of *pmt1-2 pmt2* double mutant seedlings was similar to that of *pmt1-2*, whereas the root length

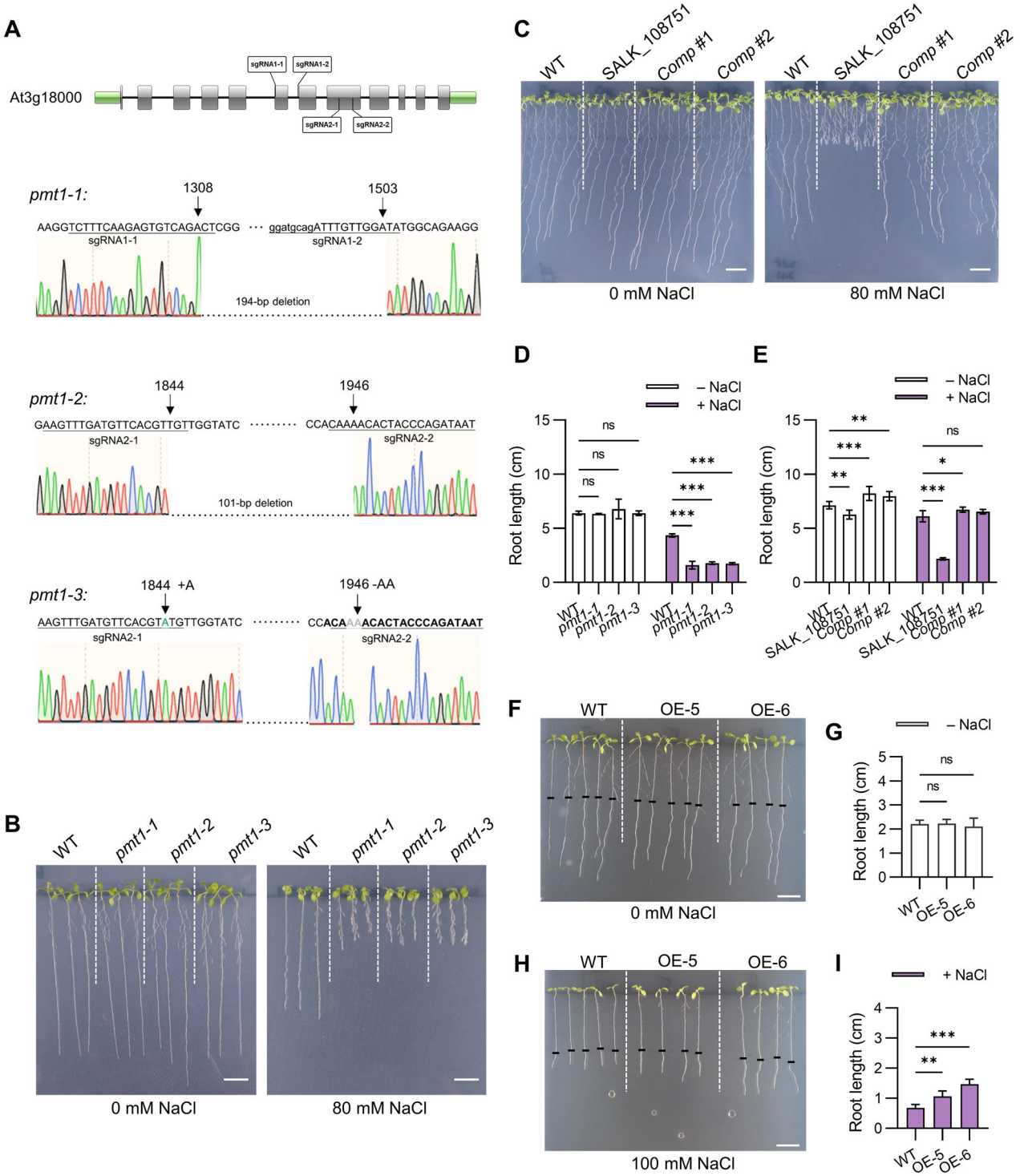

Figure 2. *PMT1* is responsible for salt tolerance

(A) Schematic illustration of two sgRNA target sites for At3g18000 (green rectangles represent UTR, gray rectangles indicate exon), and three CRISPR-*pmt1* alleles (*pmt1-1*, *pmt1-2*, *pmt1-3*) identified from T0 mutant lines. *pmt1-1* and *pmt1-2* had 194- and 101-bp deletions, respectively, *pmt1-3* had an A insertion in the 1,844 site and a two A deletion in the 1,946 site. The underline indicates the sgRNA target sequence. **(B)** Phenotype analysis of three *pmt1* mutants upon salt stress. Here, 5-d-old seedlings of wild-type (WT), *pmt1-1*, *pmt1-2*, and *pmt1-3* were transferred to 1/5 Hoagland medium with 0 mM NaCl and 80 mM NaCl. The seedlings were photographed 7 d after transfer. **(C)** PMT1 complementation recovers salt tolerance of SALK_108751. Here, 5-d-old seedlings of WT, SALK_108751, *Comp #1*, and *Comp #2* were transferred to 1/5 Hoagland medium with 0 mM NaCl and 80 mM NaCl. The seedlings were photographed 7 d after transfer. **(D)** Root length of seedlings in **(B)**, values are means ± *SD* ($n = 3$). **(E)** Root length of seedlings in **(C)**, values are means ± *SD* ($n = 8$). **(F–I)** Overexpression of *PMT1* enhanced salt tolerance. **(F)** and **(H)** The phenotype of 5-d-old of WT, OE-5, OE-9 treated without **(F)** or with **(H)** 100 mM NaCl for 7d. **(G)** and **(I)** Root length of seedlings in **(F)** and **(H)**, respectively. Bars in (**B**), (**C**), (**F**) and (**H**) = 1 cm.

of *pmt2 pmt3* was the same as in the WT (Figure S7A, B). Therefore, we concluded that PMT2 is not redundant with PMT1 in primary root development under salt stress. Based on the lack of additional phenotypes in the *pmt1-2 pmt3* double mutant relative to the *pmt1-2* single mutant, we focused on *pmt1* single mutants from this point forwards.

We also investigated whether salt stress might regulate *PMT1* expression. *PMT1* was the most highly expressed among PMT genes in roots. The expression of *PMT1* in roots increased by ~50% after 48 h of NaCl treatment and by ~66% after 120 h (Figure S6G–J). By contrast, *PMT2* expression levels did not change in response to salt treatment until 120 h, at which point transcript levels increased by ~23%, whereas *PMT3* expression decreased by ~57% (Figure S6G–J). We also examined the effects of salt stress on PMT1 protein abundance using the *ProPMT1:PMT1-GFP* transgenic line and an anti-GFP antibody. We determined that PMT1 protein levels increased upon salt treatment in roots, as evidenced by the four-fold increase in GFP fluorescence (Figure S6K, L). Immunoblot analysis confirmed the rise in PMT1 protein levels after salt treatment (Figure S6M).

The loss of PMT1 affects root meristem activity but not K^+/Na^+ homeostasis

Salt stress typically causes the replacement of K^+ by Na^+, resulting in a reduced K^+/Na^+ ratio (Sun et al., 2010; Yuan et al., 2015). To examine the underlying basis of PMT1-mediated salt tolerance, we measured Na^+ and K^+ contents in the roots and shoots of WT and *pmt1* seedlings. Under control growth conditions, we noticed no difference for K^+ contents between WT and mutant roots; however, less Na^+ accumulated in mutant roots compared with WT, resulting in a higher K^+/Na^+ ratio in the mutant roots relative to WT. We also observed no difference in Na^+ contents, K^+ contents, and the K^+/Na^+ ratio between WT and mutant shoots (Figure 3A–C). After a 5-d exposure to 80 mM NaCl, we detected no differences in Na^+ contents, K^+ contents, or K^+/Na^+ ratio in either the root or the shoot between WT and mutants (Figure 3A–C). Consistent with the finding that SALK_108751 is hypersensitive to 40 mM NaCl and 40 mM KCl (Figure S2E, F), we also observed no differences in the K^+/Na^+ ratio between WT and *pmt1*, suggesting that PMT1-mediated salt tolerance does not affect K^+/Na^+ homeostasis.

The defect in root growth of *pmt1* mutants prompted us to investigate the role of PMT1 in regulating root meristem activity in response to salt stress. Under normal growth conditions, there was no significant difference between WT and *pmt1-1* or *pmt1-2* for either MZ length or cell number (Figure S8A, B). Notably, after a 2-d exposure to salt stress, *pmt1-1* and *pmt1-2* mutant seedlings showed a shorter MZ and fewer MZ cells compared with the WT (Figure S8A, B), indicating that the loss of PMT1 function impairs root meristem activity under salt stress conditions. To confirm the importance of PMT1 in maintaining meristem activity, we introduced the *CYCB1;1:GUS* (with the *Cyclin B1;1* promoter driving the transcription of the *β-GLUCURONIDASE* reporter gene) reporter into the WT and the *pmt1-2* mutant. The *CYCB1;1* gene is a marker of the G2/M phase of the cell cycle (Wang et al., 2011). In agreement with the MZ phenotypes of the *pmt1-2* mutant, GUS activity was much lower in *pmt1-2* than in the WT under salt stress (Figure S8C), suggesting that PMT1 is involved in regulating cell division under salt stress conditions. As the activity of the root meristem is also closely related to auxin signaling (Dello Ioio et al., 2008; Hashem et al., 2021), we introduced the auxin output reporter *DR5:GUS* into *pmt1-2*. GUS staining showed that the *DR5* promoter activity was slightly lower in the root tip but higher in the stele under salt stress relative to the WT (Figure S8D, E),

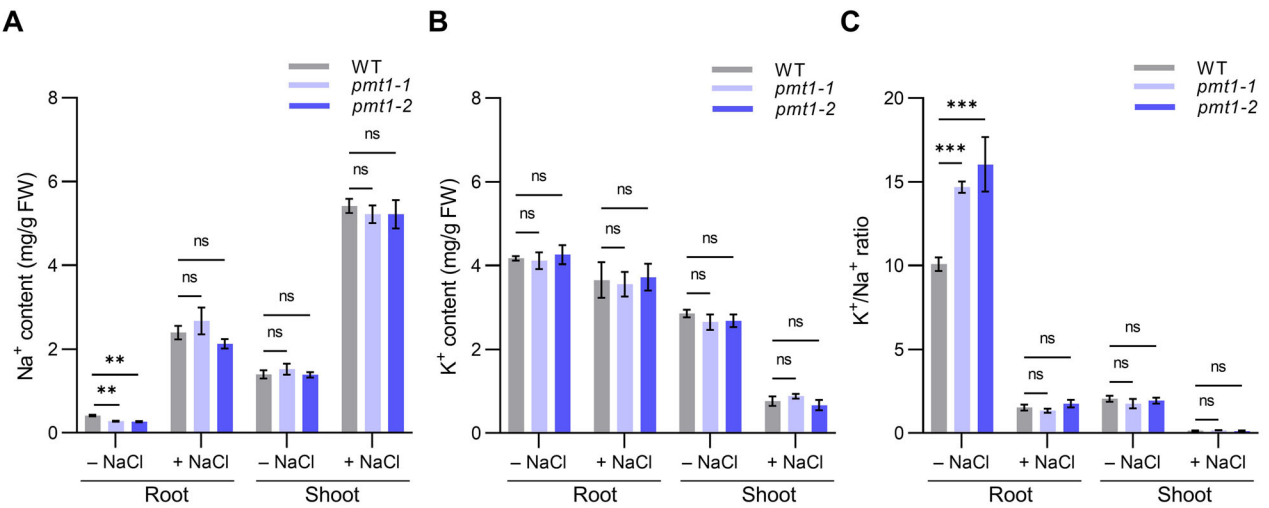

Figure 3. PMT1 mutation not K^+/Na^+ homeostasis

(A–C) Na^+ content, K^+ content, and K^+/Na^+ ratio analysis. Here, 5-d-old seedlings of WT, *pmt1-1*, and *pmt1-2* in 1/5 Hoagland medium treated with or without 80 mM NaCl for 5 d. Data presented are means ± *SD* ($n = 4$). Statistical analysis was performed using Student's *t*-test (ns, not significant; $^*P < 0.05$; $^{**}P < 0.01$; $^{***}P < 0.001$).

indicating that the *PMT1* mutation caused impaired polar auxin transport along the root apex.

PMT1 confers salt tolerance by regulating glycerolipid metabolism

PMT1 was reported to be essential for PC biosynthesis (Liu et al., 2019), which is a critical component of cell membranes. Propidium iodide staining could not only indicate dead cell (Liu et al., 2019), but also be used as an indicator for membrane damage (Graça da Silveira et al., 2002; De Calignon et al., 2009). As showed in Figure S9A, both epidermal and cortical cells of the elongation zone showed extensive staining in the mutant compared with WT seedlings under salt treatment, pointing to more severely impaired membrane in *pmt1* (Figure S9A). To determine whether the reduced root elongation of *pmt1* under 80 mM NaCl treatment was caused by lower levels of glycerolipids, we added soybean lecithin that contained various glycerolipids, such as PC, phosphatidylglycerol (PG), phosphatidylinositol (PI), and phosphatidic acid (PA), to growth medium containing NaCl. Notably, soybean lecithin fully restored the root growth of *pmt1* to the levels seen in WT seedlings (Figure S9B, C).

We also measured glycerolipid content in the roots of WT and *pmt1-2* seedlings treated with 80 mM NaCl for 5 d or maintained on normal growth medium. With the exception of PE, other major classes of plant membrane phospholipids (PC, PG, phosphatidylserine [PS], and PI) showed no difference in their contents between the WT and *pmt1-2* under control conditions (Figure 4A). However, we observed a modest reduction only in PC contents in *pmt1-2* upon exposure to 80 mM NaCl compared with the WT (Figure 4A). Moreover, we determined that the relative change of PC, PE, and PS contents in *pmt1-2* was greater than that in the WT (Figure S10A).

Monogalactosyldiacylglycerol (MGDG) and digalactosyldiacylglycerol (DGDG) are the two nonionic lipid constituents of the thylakoid membrane in land plants, whereas sulfoquinovosyldiacylglycerol (SQDG) is a minor component that provides the lipid matrix with a negatively charged lipid–water interface (Douce and Joyard, 1996). MGDG was shown to improve salt tolerance by maintaining the structure and function of tobacco (*Nicotiana tabacum*) plant cell membranes (Wang et al., 2014). We detected no difference in DGDG or SQDQ contents between the WT and *pmt1-2*, but MGDG contents were both lower in *pmt1-2* with or with salt treatment (Figure 4B), suggestive of lipid remodeling in nonplastidic and plastidic membranes in *pmt1-2*. Moreover, there was no significant change in the trend of MGDG, DGDG, and SQDG levels after salt stress between the WT and *pmt1-2* (Figure S10B).

DAG is not only the substrate for the biosynthesis of membrane lipids such as PC and PE, but it is also the branch point between the biosynthesis of membrane lipids and triacylglycerol (TAG) storage lipids (Chen et al., 2018). We noticed a more prominent relative change for TAG or DAG in *pmt1-2* after salt stress compared with that seen in the WT (Figure S10C). and observed an increase in TAG contents in *pmt1-2* upon salt treatment relative to the WT, whereas DAG contents were comparable between the two genotypes (Figure 4C), suggesting that DAG is preferentially utilized to biosynthesize storage lipids in *pmt1-2* during salinity stress, therefore resulting in the reduction of PC.

Phosphatidic acid was reported to be produced mainly via hydrolysis of structural glycerophospholipids such as PC and PE through phospholipase D (PLD) or by conversion of phosphoinositides via phospholipase C (PLC) to form DAG, which is itself converted to PA by diacylglycerol kinase (DGK) (Saucedo-García et al., 2015). Consistent with the reduced PC levels seen in the *pmt1-2* mutant, the content of PA increased significantly in *pmt1-2* after salt stress (Figure 4D). These results suggested that PMT1-mediated glycerolipid metabolism is critical for salt tolerance.

ABA regulated the expression of *PMT1* under salt stress

To examine how *PMT1* transcription was regulated by salt stress, we carried analyzed *cis*-elements in the *PMT1* promoter using Plant CARE, which identified five ABA-responsive elements (ABREs) (Figure S11A, B). Moreover, an analysis of the JASPAR database according to Mathelier et al. (2016) resulted in the identification of several potential transcriptional regulators of *PMT1*, most of which were transcription factors involved in ABA signaling such as ABF2 (ABRE-BINDING FACTOR 2), ABF3, ABF5, ABI3 (ABA-INSENSITIVE 3), ABI4, and ABI5. We confirmed the activation of PMT1 transcription by ABI4, ABI4, and ABF3 via a dual-luciferase reporter system, in which the firefly luciferase (*LUC*) reporter gene was placed under the control of a 1,609-bp fragment of the *PMT1* promoter (Figure S11C). These findings pointed to the role of ABA in the regulation of *PMT1* transcription.

To directly assess the role of ABA in inducing *PMT1* expression, we determined ABA contents of WT and *pmt1-2* seedlings grown under normal conditions or exposed to NaCl treatment. The two genotypes accumulated the same levels of ABA in control conditions, but we detected ~15% ABA increase in *pmt1-2* compared with in the WT upon exposure to salt stress (Figure S12). We also investigated the effect of exogenously supplying ABA on *PMT1* expression. The application of 10 μM ABA induced *PMT1* expression by 68% relative to controls, inhibited *PMT2* very modestly, and fully repressed *PMT3* expression, although it should be noted that *PMT3* transcript levels were very low even under control conditions (Figure 5A). We independently validated the induction of *PMT1* transcription in the root by ABA with the *ProPMT1:GUS* reporter line after ABA treatment (Figure 5B, C). In addition, PMT1 protein abundance increased following treatment with exogenous ABA (Figures 5E, F, S6M). Finally, we examined *PMT1* transcript levels in mutants related to ABA biosynthesis (*aba2-1-T*) or signaling (*pyr1 prl1 pyl2 pyl4 pyl5 pyl8* sextuple mutant (*pyl112458-T*)). Relative *PMT1* transcript levels increased in the WT upon salt stress relative

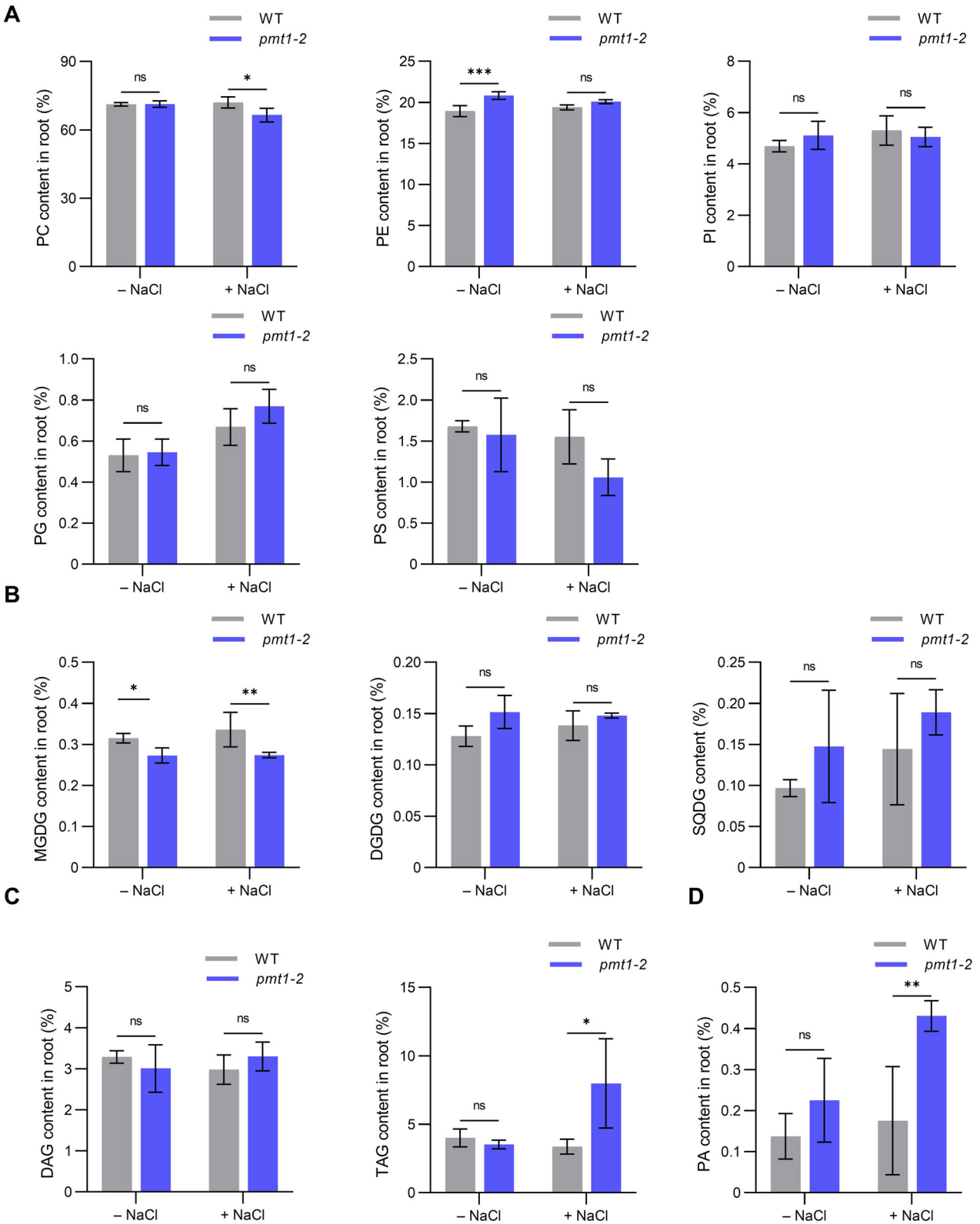

Figure 4. Polar glycerolipid contents in wild-type (WT) and *pmt1-2* with or without NaCl treatment

(A) Phospholipids including phosphatidylcholine (PC), phosphatidylethanolamine (PE), phosphatidylglycerol (PG), phosphatidylinositol (PI), and phosphatidylserine (PS). **(B)** Acylglycerols including monogalactosyldiacylglycerol (MGDG), digalactosyldiacylglycerol (DGDG), and sulfoquinovosyldiacylglycerol (SQDG). **(C)** Diacylglycerol (DAG), and triacylglycerol (TAG). **(D)** Phosphatidic acid (PA) were shown by glycerolipid composition in total lipid content (%). Polar glycerolipid profiles in the roots of 5-d-old seedlings of WT and *pmt1-2* after 5 d treatment with or without 80 mM NaCl. Values are means ± *SD* (for WT, $n = 3$; for *pmt1-2*, $n = 4$). Statistical analysis was performed using Student's *t*-test (ns, not significant; $^{*}P < 0.05$; $^{**}P < 0.01$; $^{***}P < 0.001$).

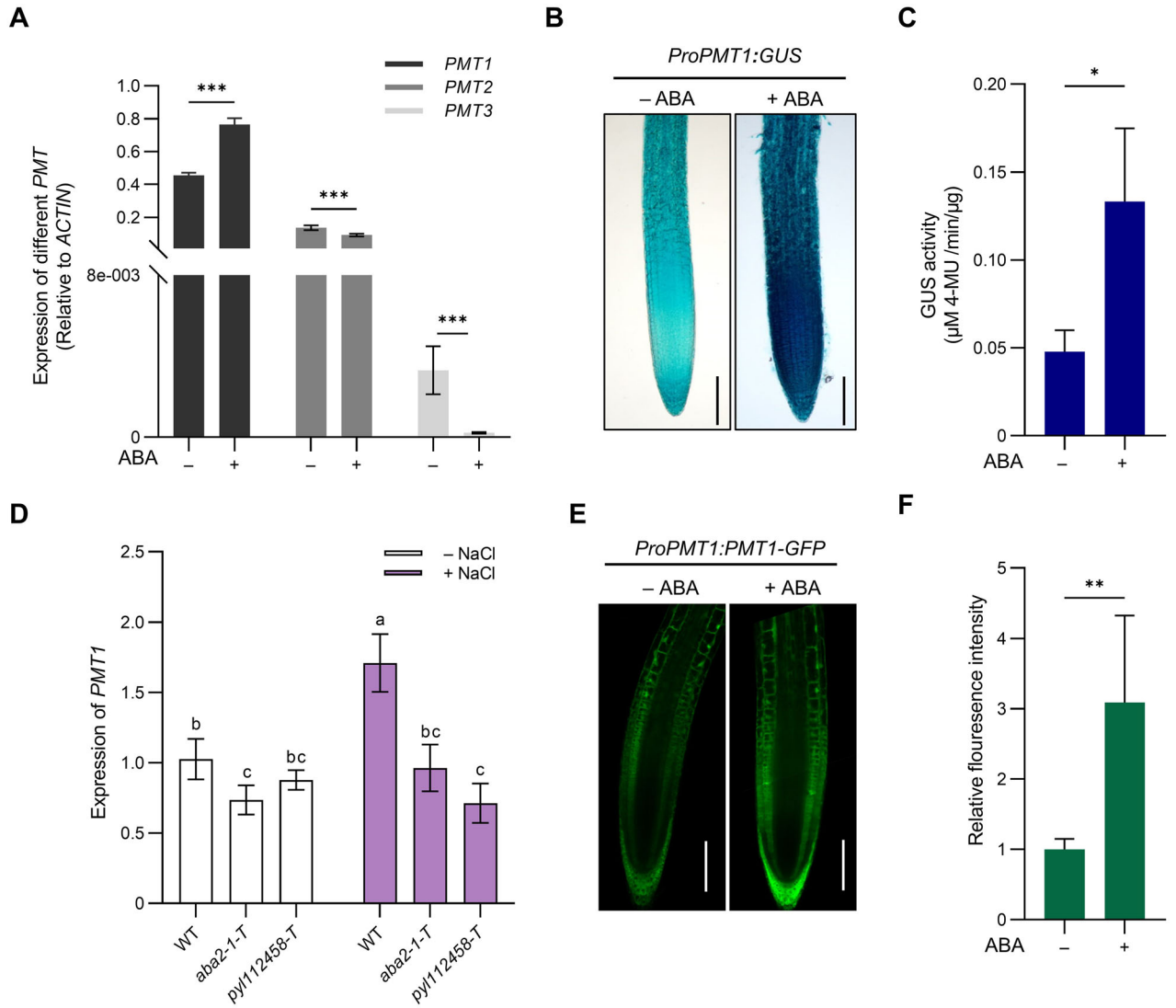

Figure 5. Abscisic acid (ABA) is required for salt-induced PMT1 accumulation

(A) Expression regulation of three *PMT* genes by ABA. Here, 5-d-old seedlings of wild-type (WT) were treated with or without 10 μM ABA. *ACTIN* was used as the internal control. Values are means ± *SD* ($n = 3$). ***$P < 0.001$ using Student's *t*-test. **(B)** GUS staining of *PMT1* expression. Here, 5-d-old *ProPMT1:GUS* transgenic plants were treated with or without 10 μM ABA. Bars = 100 μm. **(C)** GUS activity of *ProPMT1:GUS* transgenic plants treated with or without 10 μM ABA. Values are means ± *SD* ($n = 3$). *$P < 0.05$ using Student's *t*-test. **(D)** Expression of *PMT1* in WT, *aba2-1-T*, and *pyl112458-T* plants. Here, 5-d-old seedlings were treated with or without NaCl for 48 h. Values are means ± *SD* ($n = 3$). Different letters indicate significant differences using two-way ANOVA with Tukey's multiple comparison test ($P < 0.05$). **(E, F)** ABA-induced PMT1 protein accumulation. Here, 5-d-old *ProPMT1:PMT1-GFP* transgenic plants were treated with or without 10 μM ABA, and GFP proteins were observed by confocal laser microscopy. Bars = 200 μm. **(E)** Quantification of PMT1-GFP in the root with or without 80 mM NaCl treatment for 48 h ($n = 5$). **$P < 0.01$ using Student's *t*-test.

to control conditions, whereas *PMT1* expression was not significantly induced by salt stress in the ABA-related mutants (Figure 5D). These results suggested that ABA signaling is required for salt stress-induced *PMT1* expression.

PMT1 is required for ABA-regulated salt tolerance

We wished to explore the role of ABA in salt stress in *pmt1* mutants. Exogenous ABA dramatically inhibited root growth of *pmt1* mutants, whereas ABA had no effect in WT seedlings (Figure 6A, B). We hypothesized that ABA might mimic NaCl stress to affect cell division and the root auxin response. As with salt stress, ABA treatment decreased cell divisions, as seen by the lower GUS staining from the *CYCB1;1::GUS* reporter seen in *pmt1-2* compared with WT seedlings (Figure S13A). We also observed a reduction in GUS activity derived from the *DR5:GUS* reporter in the root tips of the *pmt1-2* mutant compared with the WT after 3 d of ABA treatment (Figure S13B, C). However, GUS staining from the *DR5:GUS* reporter increased in the stele of the *pmt1-2* mutant upon ABA treatment (Figure S13B, C). Therefore, our results suggested that ABA and PMT1 regulate the salt stress response.

Next, we crossed the *pmt1-2* and *aba2-1* mutants to obtain the *pmt1-2 aba2-1* double mutant (Figure S14).

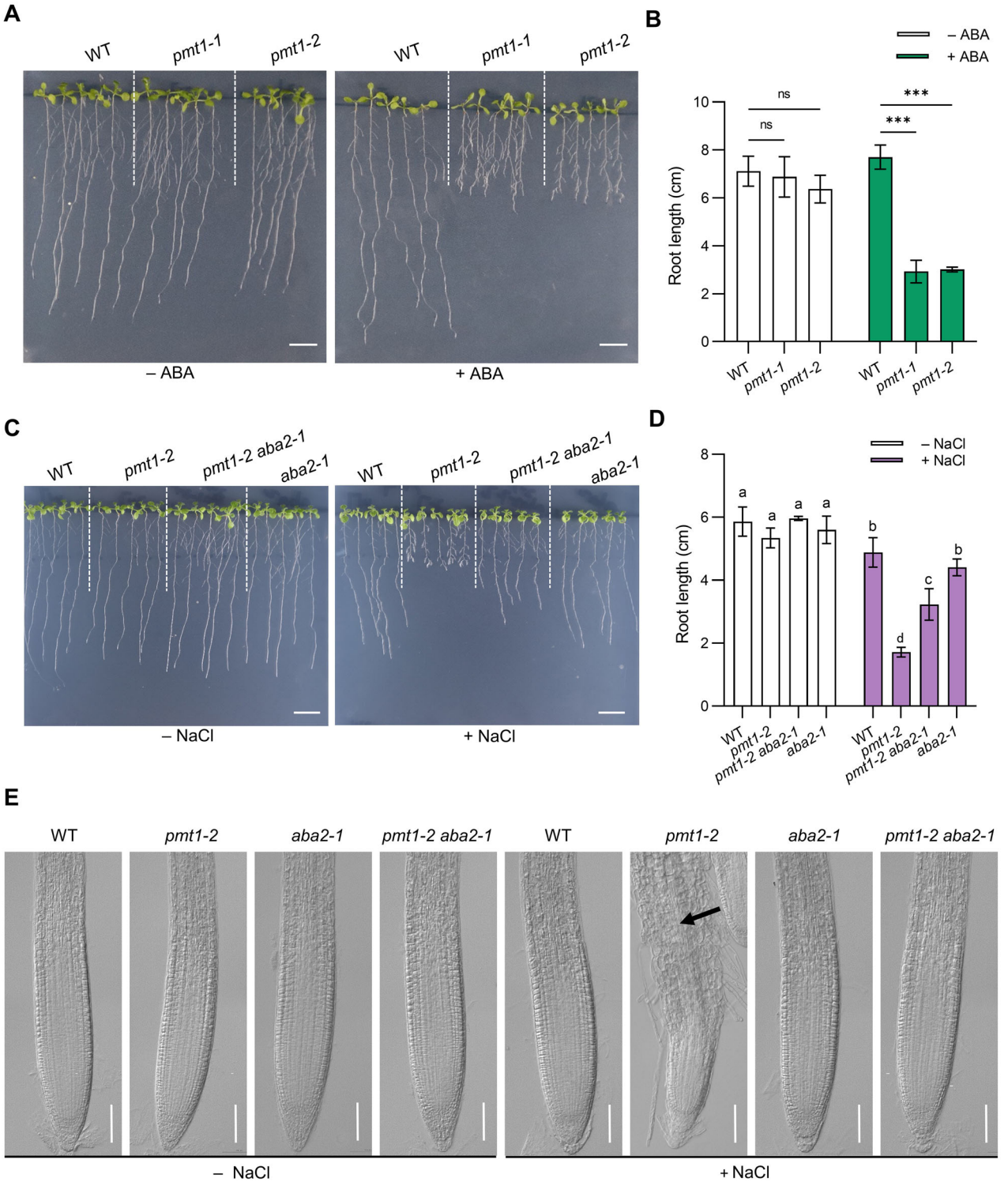

Figure 6. Hypersensitivity of *pmt1* is dependent on abscisic acid (ABA)

(A) Phenotype analysis of *pmt1* mutants to ABA. Here, 5-d-old seedlings of wild-type (WT), *pmt1-1*, and *pmt1-2* were treated with or without 10 μM ABA for 7 d. Bars = 1 cm. **(B)** Root length measurement of 5-d-old WT, *pmt1-1*, and *pmt1-2* in **(A)**. Values are the means ± *SD* ($n = 5$). Values were analyzed using Student's *t*-test (ns, not significant; ***$P < 0.001$). **(C)** Seeds of WT, *pmt1-2*, *pmt1-2 aba2-1*, and *aba2-1* germinated on 1/5 Hoagland medium for 5 d, then transferred to 1/5 Hoagland medium with or without 80 mM NaCl, the seedlings were photographed on d 7 after transfer, and the root length was measured and shown in **(D)**, values are means ± *SD* ($n = 5$). Bars = 1 cm. Letters indicate significant differences by two-way ANOVA with Tukey's multiple comparison test ($P < 0.05$). **(E)** Differential interference contrast (DIC) images showing primary roots of WT, *pmt1-2*, *pmt1-2 aba2-1*, and *aba2-1* in **(C)**, $n = 5$, the morphology of *pmt1-2* after NaCl treatment was 100% abnormal, other plants were 100% normal with or without NaCl treatment, Black arrow indicates first protoxylem element. Bars = 100 μm.

Compared with the *pmt1-2* single mutant, the *pmt1-2 aba2-1* double mutant showed a complete rescue of the salt stress-induced swelling and epidermis rupture characteristics of the *pmt1-2* single mutant (Figure 6E); in addition, root elongation also partially recovered under salt stress conditions (Figure 6C, D). We also knocked out *ABA2* in the initial SALK_108751 line by CRISPR/Cas9-mediated gene editing, resulting in the SALK_108751 *aba2-1*-C and SALK_108751 *aba2-2*-C double mutants. The root growth of the double mutants was also largely recovered upon salt stress compared with SALK_108751 (Figure S15A–D). These results indicated that the salt hypersensitivity of *pmt1* mutants is attributed to higher ABA.

ROS induced by ABA contributes to the salt sensitivity phenotype of *pmt1*

High salinity induces ROS production, which leads to damage to plant cellular structures (Noctor and Foyer, 1998), raising the possibility that the phenotypes seen in *pmt1* are caused by higher ROS accumulation. To test this hypothesis, we applied 1 mM glutathione (GSH) as an antioxidant to growth medium containing 80 mM NaCl. The addition of 1 mM GSH slightly improved the root elongation of *pmt1-1* and *pmt1-2* seedlings, it significantly inhibited the elongation of WT roots by approximately 50% under salt stress conditions (Figure 7A, B). We concluded that GSH has a very limited effect in alleviating the salt-induced root growth inhibition of *pmt1* mutants. ROS distribution has an important role in regulating cell status (Owusu-Ansah and Banerjee, 2009; Yamada et al., 2020). We therefore localized O_2^- and H_2O_2 via nitroblue tetrazolium (NBT) and 3,3′-diaminobenzidine (DAB) staining, respectively. NBT staining revealed no significant difference between the WT and *pmt1-1* or *pmt1-2* under control conditions. Notably, O_2^- accumulation was confined to the distal region of the meristematic zone in *pmt1-1* and *pmt1-2* and spread to the stele, which was not seen in WT seedlings (Figure 7C). The distribution and contents for H_2O_2 were comparable between WT and mutant seedlings under control conditions. However, after 2 d of NaCl exposure, more H_2O_2 accumulated in the stele of *pmt1* mutants, but not in the root meristematic zone (Figure 7D). These results indicated that ROS distribution was impaired in *pmt1* mutants subjected to salt stress, which may explain why exogenous GSH only modestly recovered the short root phenotype of *pmt1* mutants.

ABA was reported to induce ROS production through the oxidoreductases RESPIRATORY BURST OXIDASE HOMOLOGUE D (RbohD) and RbohF (Kwak et al., 2003); moreover, the accumulation of ROS in *abo8-1* root tips was enhanced by ABA treatment (Yang et al., 2014). We wondered whether lowering ABA contents in *pmt1* might alleviate salt-induced ROS accumulation. We therefore analyzed the *pmt1-2 aba2-1* double mutant generated above, as *aba2-1* was defective in ABA biosynthesis, and determined that both DAB and NBT staining patterns in *pmt1-2 aba2-1* were comparable with those of WT seedlings after salt treatment (Figure 7E, F). Moreover, the location of premature protoxylem differentiation moved further up in *pmt1-2 aba2-1* roots compared with those from the *pmt1-2* single mutant (Figure 7F), suggesting that PMT1 is involved in maintaining ABA-dependent ROS distribution upon salt stress.

DISCUSSION

In this study, we demonstrated that PMT1 is important for maintaining root growth under salt stress. Although the role of PMT1 in plant root development and epidermal cell integrity has been previously reported (Chen et al., 2018, 2019; Zou et al., 2019), we show that the loss of PMT1 function is associated with an extremely short root under salt stress conditions, whereas the overexpression of *PMT1* increased salt tolerance (Figures 1, 2). Moreover, we established that the role of PMT1 in salt tolerance was not associated with an imbalance of the K^+/Na^+ ratio (Figures 3A–C, S2D–F), suggesting that the mechanism underlying PMT1-mediated salt tolerance is distinct from previously reported examples. In addition, PMT1 appears to play a dominant role in salt tolerance over its two other paralogs, as we only observed hypersensitivity to salt stress in the *pmt1* single mutant and not in the *pmt2*, *pmt3, or pmt2 pmt3* mutants, and PMT2 is not redundant with PMT1 in primary root development under salt stress. (Figures 2B, D, 3E, F, S6).

We present evidence that PMT1-mediated salt tolerance is closely related to its role in lipid metabolism. First, exogenous feeding with ChoCl or lecithin rescued the *pmt1* root growth defect; together with the lower PC contents measured in *pmt1* mutants under salt stress conditions, these results suggest that PMT1 regulates salt tolerance via phospholipid metabolism (Figures S4A–H, S6A, B, 4A). Second, we demonstrate that PMT1 is a major player in maintaining membrane integrity and cell division upon salt stress. PC has been implicated in coordinating endomembrane biogenesis and cell cycle progression (Craddock et al., 2017), which is essential for forming membranes prior to division (Jackowski, 1996) and for sustaining the growth of the apical root meristem to continuously generate an elongation/differentiation zone (Perilli et al., 2012). The proposed roles for PC in plant development are therefore consistent with the severe damage seen in *pmt1* mutants for membranes in the elongation zone and the reduced root meristem activity due to the reduction of PC levels under salt stress. Finally, our results show that PMT1-mediated glycerolipid metabolism is essential for lateral root development during salt stress. Auxin modifies cell fate and activates cell division during lateral root initiation (Péret et al., 2009), and auxin polar transport is controlled by influx transporters AUX-LAX and efflux transporters PIN-FORMED (PIN) and P-GLYCOPROTEIN (PGP) (Kramer and Bennett, 2006; Vanneste and Friml, 2009). PA is required for the normal cycling of PIN-containing vesicles and for auxin transport and distribution, and therefore auxin responses (Li and Xue, 2007; Gao et al., 2013). Here, we

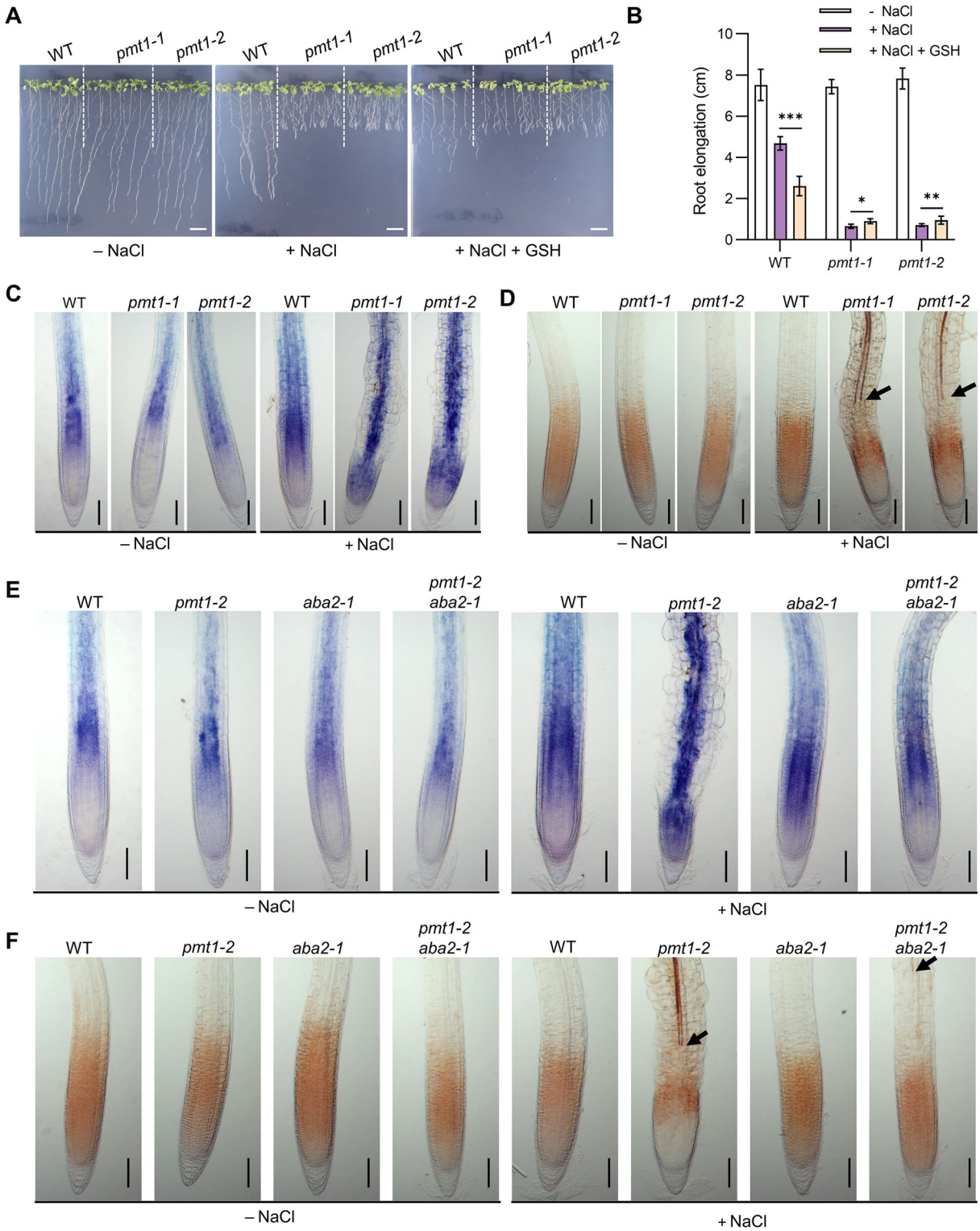

Figure 7. PMT1 attenuates abscisic acid (ABA)-induced oxidative stress upon salt stress

(A, B) Antioxidant glutathione (GSH) plays a minor role in alleviating salt sensitivity of *pmt1* mutants. **(A)** Phenotype analysis of GSH on salt sensitivity of *pmt1* mutants. Here, 5-d-old seedlings were treated without (–NaCl) or with (+) 80 mM NaCl or with 80 mM NaCl and 1 mM GSH for 7 d. **(B)** Root elongation of WT, *pmt1-1* and *pmt1-2* in **(A)**. Bars = 1 cm. Values are means ± *SD* ($n = 5$). $^{*}P < 0.05$; $^{**}P < 0.01$; $^{***}P < 0.001$ using Student's *t*-test. **(C, D)** Reactive oxygen species (ROS) measurement. **(C)** Nitroblue tetrazolium (NBT) staining for O_2^-. **(D)** 3,3′-Diaminobenzidine (DAB) staining for H_2O_2. Here, 5-d-old seedlings were treated with or without 80 mM NaCl for 2 d. Bars = 100 μm. **(E, F)** Salt-induced ROS abnormal distribution in *pmt1* mutant was attenuated in ABA-deficient mutant *aba2-1*. **(E)** NBT staining for O_2^-. **(F)** DAB staining for H_2O_2. Here, 5-d-old seedlings of wild-type (WT), *pmt1-2*, *pmt1-2 aba2-1*, and *aba2-1* were treated with or without 80 mM NaCl for 2 d. Bars = 100 μm. Black arrows indicate the position of the protoxylem.

established the PA levels increase in *pmt1* upon salt stress (Figure 4D), which might contribute to altered auxin responses in the stele of *pmt1* mutant roots, and therefore stimulate the early emergence of lateral root primordia (Figures 1C, S1D). In agreement with this notion, we observed a stronger auxin output signaling in the stele of *pmt1* seedlings compared with in the WT (Figure S8D, E). Notably, more ROS also accumulated in the stele of *pmt1* under salt stress conditions (Figure 7C, D).

It is also worth noting that the mutation of *PMT1* resulted in a short root phenotype under normal growth conditions in many previous studies (Chen et al., 2019; Liu et al., 2019; Zou et al., 2019). However, under our growth conditions (1/5 Hoagland solid growth medium with 0.8% agar), we did not observe any discernible effects on root growth between *pmt1* and WT seedlings in the absence of salt stress. Instead, we determined that the short root phenotype is associated with high salt concentrations in the growth environment (Figures 1A, B, 2B, D), suggesting that PMT1 is specifically involved in salt tolerance via root growth regulation. In agreement with our results, a similar observation was reported in the *t365* mutant, in which *PMT1* transcript levels are lower via antisense interference (Mou et al., 2002). We speculate that the published differences for root growth in the *pmt1* mutant across different studies may result from the combined effects of high ionic strength in the growth medium and the residual levels of PMT1 in the mutants.

We showed that *PMT1* transcript levels and PMT1 protein abundance increase in the primary root tip upon salt treatment (Figure S6I–M), which raises the question of the transcriptional regulation of *PMT1* by salt stress. The expression of *PMT1* has been previously reported to be negatively regulated by PCho via its upstream open reading frames (uORFs) (Tabuchi et al., 2006; Alatorre-Cobos et al., 2012; Craddock et al., 2015). Moreover, PMT1 transcript levels were higher in the *npc2 npc6* (*non-specific phospholipase c2* and *c6*) knockdown mutant lines with decreased PCho (Ngo et al., 2019). Considering that NPC-catalyzed production of PCho interacts with the PMT1-dependent pathway for PCho production, we hypothesize that the transcriptional induction of *PMT1* in *npc* mutants is more likely to represent a feedback regulation. In this study, we demonstrated that ABA, possibly via its signaling pathway, may be critical for the transcriptional regulation of *PMT1* under salt stress. This conclusion is based on the following lines of evidence. First, the expression of *PMT1* was induced by exogenous ABA treatment (Figure 5A–C). Second, the transcriptional induction of *PMT1* was markedly reduced in the *aba2-1* mutant under salt stress and completely blocked in the *pyl112458* sextuple mutant (Figure 5D). Finally, salt stress induced ABA accumulation (Figure S12). Notably, *PMT1* was reported to be involved in the 1-aminocyclopropane 1-carboxylic acid (ACC)-mediated control of root cell elongation in Arabidopsis (Markakis et al., 2012). Whether the regulation of *PMT1* expression by ABA is dependent on ACC deserves further investigation.

ABA plays essential roles in plant growth and development, as well as in plant adaptation to abiotic and biotic stresses (Ober and Sharp, 1994; Zhang et al., 2010; Vishwakarma et al., 2017; Fan et al., 2019; Chen et al., 2020). Surprisingly, *pmt1* mutants were hypersensitive to exogenous ABA application (Figure 6A, B). Moreover, the *pmt1-2 aba2-1* double mutant exhibited a partial rescue of the short root phenotype of *pmt1-2* under salt stress (Figure 6C, D). These results indicated that the role of ABA in salt stress is dependent on PMT1. ABA stimulates ROS production through NADPH oxidases, and higher ROS levels inhibit root cell elongation (Kwak et al., 2003). ABA-mediated ROS in mitochondria also suppressed primary root growth by controlling *PLETHORA* expression (Yang et al., 2014). Here, we showed that ROS distribution in the root apex was impaired in *pmt1* mutants experiencing salt stress (Figure 7C, D). However, this disturbance in ROS distribution was recovered by lowering cellular ABA contents, as demonstrated by the results obtained with the *pmt1-2 aba2-1* double mutant (Figure 7E, F). Therefore, PMT1 is likely to play roles in maintaining ABA-induced ROS production and distribution under salt stress conditions, which is critical for root growth.

In summary, we demonstrated that, upon salt stress exposure, *pmt1* mutant seedlings exhibited an inhibition of primary root elongation, with a shorter meristematic zone, enlarged epidermal cells, lateral roots appearing closer to the QC, lower H_2O_2 accumulation in the meristematic zone, and more O_2^- accumulation in the stele, relative to WT seedlings (Figure 8A). We propose a model (Figure 8B), in which salt stress causes the accumulation of ABA, whose signaling pathway in turn induces *PMT1* transcription and promotes the accumulation of PMT1 protein in WT seedlings. PMT1-dependent lipid biosynthesis alleviated the damage caused by salt stress such as ROS burst and membrane injury, helping seedlings maintain meristematic activity and cell membrane integrity. However, in *pmt1* seedlings, salt-induced ABA accumulation promoted ROS accumulation, which damaged cell membranes and influenced meristem activity. In addition, overexpression of *PMT1* improved root growth in a high salinity environment, providing a new perspective for improving plant tolerance to high salinity.

MATERIALS AND METHODS

Plant materials and growth conditions

Arabidopsis (*Arabidopsis thaliana*) plants used in this study were on the Columbia-0 (Col-0) background. The T-DNA insertion mutants SALK_108751, SALK_117670, and SALK_088182 were ordered from the ABRC. Surface-sterilized *Arabidopsis* seeds were sown on 1/5 Hoagland solid medium consisting of 0.4 mM $MgSO_4$, 0.2 mM $NH_4H_2PO_4$, 1 mM KNO_3, 1 mM $Ca(NO_3)_2$, 20 μM Fe-EDTA, 3 μM H_3BO_3, 0.5 μM $MnCl_2$, 0.2 μM $CuSO_4$, 0.4 μM $ZnSO_4$, $(NH_3)_6Mo_7O_2$ (Hoagland and Arnon, 1950), and 0.8% (w/v) agar, stratified at 4°C for 2 d in the dark and then transferred

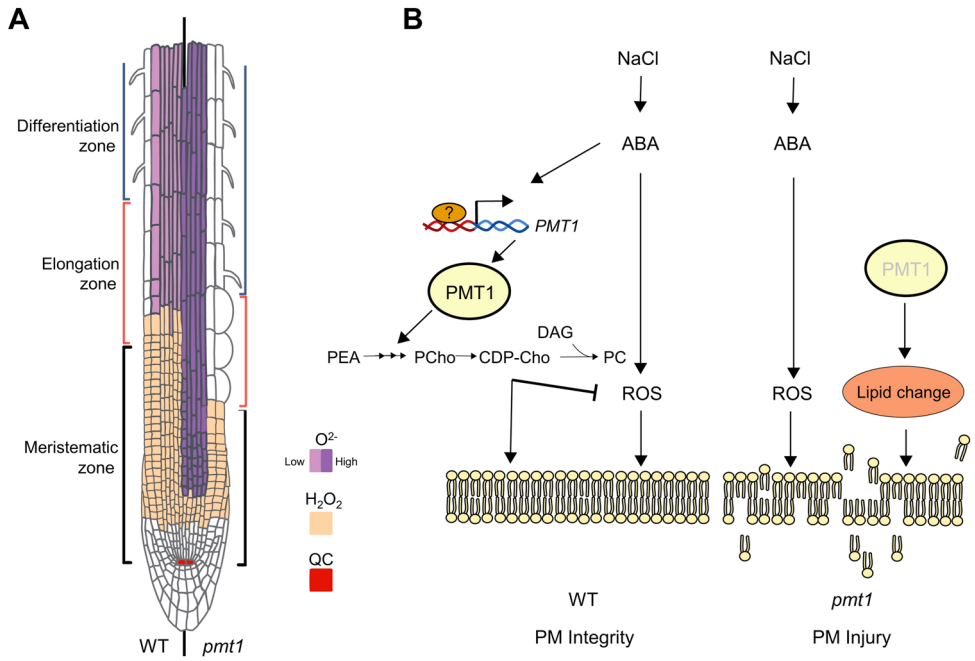

Figure 8. Model illustrating abscisic acid (ABA)-mediated PMT1 expression in salt tolerance via alleviation of ABA-induced oxidative stress

(A) Schematic model of the primary root in wild-type (WT) (left) and *pmt1* (right) after salt stress. The red square represents the position of the quiescent center (QC); light purple and deep purple indicate the low and high concentration of O_2^-, respectively; the orange color indicates H_2O_2 staining. **(B)** Salt stress triggers the production of ABA. Interestingly, ABA increases the transcription of *PMT1* and PMT1 protein accumulation in the root tip, accelerating the conversion of phosphoethanolamine (PEA) to phosphocholine (PCho), which increases the production of phosphatidylcholine (PC). Conversely, ABA also induces the production of reactive oxygen species (ROS). PMT1-dependent lipid synthesis could alleviate ROS injury, while conferring WT plant tolerance to salt stress by modulating membrane integrity. However, in the *pmt1* mutant, the generation of PCho and PC is impaired. Salt-induced ABA promotes the ROS abnormal distribution that damages the cell membrane, resulting in hypersensitivity to salt stress.

to a growth chamber at 23°C under a 16-h-light/8-h-dark photoperiod. After 5 d growth, seedlings were transferred to a new medium.

Cloning, construct generation, and plant transformation

To generate the *ProPMT1:GUS* reporter line, a 2,161-bp promoter fragment for *PMT1* was amplified from Col-0 genomic DNA and ligated into the pCAMBIA1301 (fused to the *GUS* gene). To complement the SALK_108751 mutant, a 2,751-bp genomic fragment spanning the coding region and the 2,161-bp *PMT1* promoter were cloned into the binary vector pCAMBIA1300 to generate the *ProPMT1:PMT1-GFP* construct. The *ProPMT1:GUS* and *ProPMT1:PMT1-GFP* constructs were transformed into SALK_108751. To generate transgenic lines overexpressing *PMT1*, the coding sequence of *PMT1* was PCR amplified and cloned into pCAMBIA1300, which harbors the cauliflower mosaic virus (CaMV) 35S promoter (*35S:PMT1-GFP*). To obtain gene-edited *pmt1* mutants, two CRISPR/Cas9 constructs were constructed to edit *PMT1* on the Col-0 background. The constructs for CRISPR/Cas9-mediated gene editing were designed according to a protocol described previously (Xing et al., 2014). Transgenic *Arabidopsis* plants were generated by the Agrobacterium (*Agrobacterium tumefaciens*)-mediated floral dip method (Clough and Bent, 1998), and homozygous transgenic T3 lines carrying a single insertion were selected. The primers used for plasmid construction are listed in Table S1.

Salt treatment and microscopy observations

Here, 5-d-old seedlings were transferred from control growth medium to growth medium containing 80 mM NaCl for 7 d. For choline supplementation, choline chloride (ChoCl) was added to the medium to a final concentration of 100 μM with or without 80 mM NaCl. For mannitol treatments, 200 mM mannitol was added to 1/5 Hoagland solid medium. For PEG treatment, we followed a previously published method (Verslues et al., 2006). Root elongation was measured using ImageJ software (https://imagej.nih.gov/ij/). To analyze the apoptosis of root cells and visualize cell contour, the roots were stained with propidium iodide (10 mg/mL) for 1 min and washed with deionized water for 2 min. The roots were then observed using a confocal laser scanning microscope (LSM710; Carl Zeiss, Jena, Germany). Morphological changes in the root apex were observed by DIC microscopy (ECLIPSE Ni-U; Nikon), and root meristem length was measured from the QC to the first elongated cell in the cortex using NIS-Elements BR software (https://www.microscope.healthcare.nikon.com/)

GUS staining and GUS activity measurement

Histochemical staining for GUS activity was performed with *ProPMT1:GUS* transgenic lines and *pmt1-2 DR5:GUS* and *pmt1-2 CYCB:GUS* seedlings. Seedlings were immersed in GUS staining solution (0.1 M sodium phosphate, pH 7.0, 10 mM EDTA, 0.1% [v/v] Triton X-100, 1 mM $K_3Fe(CN)_6$, 1 mg/mL X-Gluc [Yeasen]) overnight at 37°C (Jefferson, 1987). After staining, photographs were taken with a Nikon AZ100 microscope. For GUS activity measurement, roots of *ProPMT1:GUS* transgenic lines with or without treatment for 2 d were collected and then total protein was extracted using a GUS quantitative assay kit (Coolaber). Protein concentration was determined using Quick Start™ Bradford 1× Dye Reagent (Bio-Rad), and GUS activity was quantified according to the instructions.

RNA extraction, RT-PCR, and RT-qPCR

After treatment, roots were excised and immediately frozen in liquid nitrogen. Total RNA was extracted using an RNAprep pure Plant Kit (Tiangen). Reverse transcription was performed with 1 μg of total RNA using the PrimeScript™ RT Master Mix (Takara). qPCR was performed on a LightCycler480v instrument (Roche Diagnostics, Basel, Switzerland) using SYBR® Green Chemistry (Toyobo). The primer pair sequences were designed using the qPrimerDB-qPCR Primer Database (https://biodb.swu.edu.cn/qprimerdb/) and are listed in Table S1.

Na^+ and K^+ content analysis

Seedlings were exposed to 80 mM NaCl medium for 5 d or maintained on normal growth medium, and roots and shoots were harvested, weighed, and oven-dried at 65°C. After digestion with 65% (v/v) HNO_3, Na^+ and K^+ contents were determined by inductively coupled plasma mass spectrometry (IRIS/AP optical emission spectrometer; Thermo Jarrell Ash, Franklin, MA, USA) after dilution to 5.0 mL with deionized water.

ROS detection

The contents of ROS H_2O_2 and O_2^- were analyzed by DAB staining and NBT staining. Here, 5-d-old seedlings exposed to 80 mM NaCl for 2 d were incubated in DAB staining buffer (Huang et al., 2019) (0.2 mg/mL DAB dissolved in 50 mM Tris-HCl, pH 5.0) for 1.5 h or in NBT staining buffer (Zhou et al., 2012) (0.5 mg/mL NBT dissolved in 20 mM potassium phosphate, pH 6.2) for 60 min. The reaction was stopped by washing the samples with 75% (v/v) ethanol. The stained samples were cleared in chloral hydrate (1 g/mL,15% [v/v] glycerol), and images were taken on a Nikon AZ100 microscope. The relative staining intensity was analyzed using ImageJ software.

Immunoblot analysis

For total protein extraction, a RIPA lysis buffer containing 50 mM Tris-HCl pH 8.0, 150 mM NaCl, 1% (v/v) Triton X-100, 0.5% (w/v) sodium deoxycholate, 5 mM EDTA, and 10% (v/v) glycerol was used. Here, 2-d-old seedlings exposed to 80 mM NaCl or 10 μM ABA or maintained on control medium were homogenized in extraction buffer and centrifuged at 4°C for 10 min at ~13,400 *g*. The protein in the supernatants was boiled with loading buffer at 95°C for 10 min. After separation by SDS-PAGE, immunoblot analysis was performed following Xu et al. (2020). Briefly, the separated proteins were electro-transferred to a polyvinylidene fluoride membrane using the Mini Trans-Blot System (Bio-Rad). The membrane was incubated in anti-GFP or anti-actin antibody (1:4,000 dilution) for 1 h, washed with phosphate buffered saline with 0.1% (v/v) Tween-20 (PBST) three times, and then incubated with a goat anti-mouse HRP-conjugated antibody (1:4,000 dilution) for 1 h. Immunoblot signals were detected with the Luminata™ Western HRP Substrate Kit (Merck-Millipore).

ABA content measurement

Here, 5-d-old Col-0 and *pmt1-2* seedlings were exposed to 80 mM NaCl for 2 d or maintained on normal growth medium, after which their roots were collected, weighed, and immediately frozen in liquid nitrogen. ABA was extracted as described previously (González-Guzmán et al., 2002). Endogenous ABA levels were determined using a competitive ELISA kit (Cao Benyuan, NanJin).

Lipid extraction

Total lipid extraction was conducted with methyl-*tert*-butyl (MTBE) as previously described (Matyash et al., 2008). Here, 5-d-old Col-0 and *pmt1-2* seedlings grown on 1/5 Hoagland medium were exposed to 80 mM NaCl for 5 d or maintained on control growth medium before their roots were excised, frozen in liquid nitrogen immediately, and pulverized. Each sample was resuspended in 750 μL methanol and vortexed. Then, 2.5 mL MTBE was added and incubated at room temperature on a shaker for 1 h. Finally, 625 μL ddH_2O was added, and the mixture incubated for 10 min, and centrifuged at 1,000 *g* for 10 min at room temperature. The upper phase was collected and dried under nitrogen flow.

Liquid chromatography–mass spectrometry (LC-MS) analysis

Lipids were resuspended in 100 μL of a methanol/chloroform mixture (9:1, v/v). Aliquots injections (2 μL for positive mode analysis and 5 μL for negative mode analysis) of Arabidopsis root lipids were made. LC separation was performed on an Agilent 1290 Infinity II LC System, with a 19-min gradient time on a reverse phase C18 column (Agilent InfinityLab Poroshell 120 EC-C18, 3.0 × 100 mm, 2.7 μm). Mobile phase A consisted of 10 mM ammonium acetate and 0.2 mM ammonium fluoride in a 9:1 water/methanol mixture, whereas mobile phase B consisted of 10 mM ammonium acetate and 0.2 mM ammonium fluoride in a 2:3:5 acetonitrile/methanol/isopropanol mixture. Negative and positive polarity data were acquired on an Agilent 6546 LC/Q-TOF instrument using iterative MS/MS acquisition mode on six injections of extracted lipids for each polarity (Sartain et al., 2019). Detailed experimental methods for chromatography and mass spectrometry can be found in the Agilent application note 5994-0775en (Sartain et al., 2019). Two methods were used, a

high-load and a low-load method, to determine the effect of high injection volumes/concentration on the number of annotations using the Agilent 6546 LC/Q-TOF. Iterative MS/MS acquisition data for the Arabidopsis root lipids in positive and negative polarity were separately analyzed by lipidomics software platform including Lipid Annotator and the downstream workflow with Agilent software (Koelmel et al., 2020). In detail, PC, PE, TAG, and DAG were identified in positive ionization mode; phosphatidylglycerol (PG), PI, PS, MGDG, DGDG, SQDG, and PA were obtained from the negative ionization mode. The proportion of various glycerolipids in total lipids was calculated.

Statistical analysis

Statistical analysis was carried out using Student's *t*-tests or two-way analysis of variance (ANOVA) with Tukey's multiple comparison test.

Accession numbers

The accession numbers are as follows: *PMT1* (At3g18000), *PMT2* (At1g48600), and *PMT3* (At1g73600).

ACKNOWLEDGEMENTS

We thank Dr. Yang Zhao (Shanghai Center for Plant Stress Biology, CAS, China) for kindly donating the seeds of the *pyl112458-T* and *aba2-1* mutants. We also thank Dr. Pengxiang Fan (Department of Horticulture, Zhejiang University, Hangzhou) for the help in lipid analysis. This work was supported by the National Key Research and Development Program of China (Grant No. 2016YFD0100704), and Key R&D Program of Zhejiang (2022C02030).

CONFLICTS OF INTEREST

The authors declare that they have no conflicts of interest associated with this work.

AUTHOR CONTRIBUTIONS

Q.Y.H. and J.L.Y. designed the experiments, analyzed the data, and wrote the manuscript. Q.Y.H., J.F.J., F.F.D., and H. Q.L. performed the experiments. J.M.X. analyzed the elements. S.J.Z. discussed the results. All authors read and approved of the manuscript.

Edited by: Yan Guo, China Agricultural University, China

Received May 7, 2022; **Accepted** Jul. 4, 2022; **Published** Jul. 5, 2022

REFERENCES

Alatorre-Cobos, F., Cruz-Ramírez, A., Hayden, C.A., Pérez-Torres, C.A., Chauvin, A.L., Ibarra-Laclette, E., Alva-Cortés, E., Jorgensen, R.A., and Herrera-Estrella, L. (2012). Translational regulation of *Arabidopsis XIPOTL1* is modulated by phosphocholine levels via the phylogenetically conserved upstream open reading frame 30. J. Exp. Bot. **63:** 5203–5221.

Barrero, J.M., Rodríguez, P.L., Quesada, V., Piqueras, P., Ponce, M.R., and Micol, J.L. (2006). Both abscisic acid (ABA)-dependent and ABA-independent pathways govern the induction of *NCED3*, *AAO3* and *ABA1* in response to salt stress. Plant Cell Environ. **29:** 2000–2008.

Bolognese, C.P., and McGraw, P. (2000). The isolation and characterization in yeast of a gene for *Arabidopsis S*-adenosylmethionine: Phosphoethanolamin *N*-methyltransferase. Plant Physiol. **124:** 1800–1813.

Chen, K., Li, G.J., Bressan, R.A., Song, C.P., Zhu, J.K., and Zhao, Y. (2020). Abscisic acid dynamics, signaling, and functions in plants. J. Integr. Plant Biol. **62:** 25–54.

Chen, W.H., Salari, H., Taylor, M.C., Jost, R., Berkowitz, O., Barrow, R., Qiu, D.Y., Branco, R., and Masle, J. (2018). NMT1 and NMT3 *N*-methyltransferase activity is critical to lipid homeostasis, morphogenesis, and reproduction. Plant Physiol. **177:** 1605–1628.

Chen, W.H., Taylor, M.C., Barrow, R.A., Croyal, M., and Masle, J. (2019). Loss of phosphoethanolamine *N*-methyltransferases abolishes phosphatidylcholine synthesis and is lethal. Plant Physiol. **179:** 124–142.

Clough, S.J., and Bent, A.F. (1998). Floral dip: A simplified method for *Agrobacterium*-mediated transformation of *Arabidopsis thaliana*. Plant J. **16:** 735–743.

Craddock, C.P., Adams, N., Bryant, F.M., Kurup, S., and Eastmond, P. J. (2015). Phosphatidic acid phosphohydrolase regulates phosphatidylcholine biosynthesis in *Arabidopsis* by phosphatidic acid-mediated activation of CTP: Phosphocholine cytidylyltransferase activity. Plant Cell **27:** 1251–1264.

Craddock, C.P., Adams, N., Kroon, J.T.M., Bryant, F.M., Hussey, P.J., Kurup, S., and Eastmond, P.J. (2017). Cyclin-dependent kinase activity enhances phosphatidylcholine biosynthesis in *Arabidopsis* by repressing phosphatidic acid phosphohydrolase activity. Plant J. **89:** 3–14.

Cruz-Ramiérez, A., Loépez-Bucio, J., Ramiérez-Pimentel, G., Zurita-Silva, A., Saénchez-Calderon, L., Ramiérez-Chaévez, E., Gonzaélez-Ortega, E., and Herrera-Estrella, L. (2004). The *xipotl* mutant of *Arabidopsis* reveals a critical role for phospholipid metabolism in root system development and epidermal cell integrity. Plant Cell **16:** 2020–2034.

De Calignon, A., Spires-Jones, T.L., Pitstick, R., Carlson, G.A., and Hyman, B.T. (2009). Tangle-bearing neurons survive despite disruption of membrane integrity in a mouse model of tauopathy. J. Neuropathol. Exp. Neurol. **68:** 757–761.

Dello Ioio, R., Nakamura, K., Moubayidin, L., Perilli, S., Taniguchi, M., Morita, M.T., Aoyama, T., Costantino, P., and Sabatini, S. (2008). A genetic framework for the control of cell division and differentiation in the root meristem. Science **322:** 1380–1384.

Douce, R., and Joyard, J. (1996). Biosynthesis of thylakoid membrane lipids. In: D.R. Ort, C.F. Yocum, I.F. Heichel, eds. *Oxygenic Photosynthesis: The Light Reactions*. Dordrecht, the Netherlands: Springer. pp. 69–101.

Fan, W., Xu, J.M., Wu, P., Yang, Z.X., Lou, H.Q., Chen, W.W., Jin, J.F., Zheng, S.J., and Yang, J.L. (2019). Alleviation by abscisic acid of Al toxicity in rice bean is not associated with citrate efflux but depends on ABI5-mediated signal transduction pathways. J. Integr. Plant Biol. **61:** 140–154.

Feng, W., Kita, D., Peaucelle, A., Cartwright, H.N., Doan, V., Duan, Q. H., Liu, M.C., Maman, J., Steinhorst, L., Schmitz-Thom, I., Yvon, R., Kudla, J., Wu, H.M., Cheung, A.Y., and Dinneny, J.R. (2018). The FERONIA receptor kinase maintains cell-wall integrity during salt stress through Ca^{2+} signaling. Curr. Biol. **28:** 666–675.

Gao, H.B., Chu, Y.J., and Xue, H.W. (2013). Phosphatidic Acid (PA) binds PP2AA1 to regulate PP2A activity and PIN1 polar localization. Mol. Plant **6:** 1692–1702.

González-Guzmán, M., Apostolova, N., Bellés, J.M., Barrero, J.M., Piqueras, P., Ponce, M.R., Micol, J.L., Serrano, R., and Rodríguez, P.L. (2002). The short-chain alcohol dehydrogenase ABA2 catalyzes the conversion of xanthoxin to abscisic aldehyde. Plant Cell **14:** 1833–1846.

Graça da Silveira, M., Vitória San Romão, M., Loureiro-Dias, M.C., Rombouts, F.M., and Abee, T. (2002). Flow cytometric assessment of membrane integrity of ethanol-stressed oenococcus oeni cells. Appl. Environ. Microbiol. **68:** 6087–6093.

Hashem, A.M., Moore, S., Chen, S.J., Hu, C.C., Zhao, Q., Elesawi, I.E., Feng, Y.N., Topping, J.F., Liu, J.L., Lindsey, K., and Chen, C.L. (2021). Putrescine depletion affects *Arabidopsis* root meristem size by modulating auxin and cytokinin signaling and ROS accumulation. Int. J. Mol. Sci. **22:** 4094.

Hoagland, D.R., and Arnon, D.I. (1950). The water-culture method for growing plants without soil. Calif. Agric. Exp. Stn. **347:** 1–32.

Huang, L., Yu, L.J., Zhang, X., Fan, B., Wang, F.Z., Dai, Y.S., Qi, H., Zhou, Y., Xie, L.J., and Xiao, S. (2019). Autophagy regulates glucose-mediated root meristem activity by modulating ROS production in *Arabidopsis*. Autophagy **15:** 407–422.

Jackowski, S. (1996). Cell cycle regulation of membrane phospholipid metabolism. J. Biol. Chem. **271:** 20219–20222.

Jefferson, R.A. (1987). Assaying chimeric genes in plants: The *GUS* gene fusion system. Plant Mol. Biol. Report **5:** 387–405.

Jost, R., Berkowitz, O., Shaw, J., and Masle, J. (2009). Biochemical characterization of two wheat phosphoethanolamine *N*-methyltransferase isoforms with different sensitivities to inhibition by phosphatidic acid. J. Biol. Chem. **284:** 31962–31971.

Kamiyama, Y., Hirotani, M., Ishikawa, S., Minegishi, F., Katagiri, S., Rogan, C.J., Takahashi, F., Nomoto, M., Ishikawa, K., Kodama, Y., Tada, Y., Takezawa, D., Anderson, J.C., Peck, S.C., Shinozaki, K., and Umezawa, T. (2021). *Arabidopsis* group C raf-like protein kinases negatively regulate abscisic acid signaling and are direct substrates of SnRK2. Proc. Natl. Acad. Sci. U.S.A. **118:** e2100073118.

Kennedy, E.P., and Weiss, S.B. (1956). Function of cytidine coenzymes in the biosynthesis of phospholipides. J. Biol. Chem. **222:** 193–213.

Koelmel, J.P., Li, X., Stow, S.M., Sartain, M.J., Murali, A., Kemperman, R., Tsugawa, H., Takahashi, M., Vasiliou, V., Bowden, J.A., Yost, R. A., Garrett, T.J., and Kitagawa, N. (2020). Lipid annotator: Towards accurate annotation in non-targeted liquid chromatography high-resolution tandem mass spectrometry (LC-HRMS/MS) lipidomics using a rapid and user-friendly software. Metabolites **10:** 101.

Kramer, E.M., and Bennett, M.J. (2006). Auxin transport: A field in flux. Trends Plant Sci. **11:** 382–386.

Kwak, J.M., Mori, I.C., Pei, Z.M., Leonhardt, N., Torres, M.A., Dangl, J. L., Bloom, R.E., Bodde, S., Jones, J.D.G., and Schroeder, J.I. (2003). NADPH oxidase *AtrbohD* and *AtrbohF* genes function in ROS-dependent ABA signaling in *Arabidopsis*. EMBO J. **22:** 2623–2633.

Li, G., and Xue, H.W. (2007). *Arabidopsis PLD*ζ*2* regulates vesicle trafficking and is required for auxin response. Plant Cell **19:** 281–295.

Liu, Y.C., Lin, Y.C., Kanehara, K., and Nakamura, Y. (2018). A pair of phospho-base methyltransferases important for phosphatidylcholine biosynthesis in *Arabidopsis*. Plant J. **96:** 1064–1075.

Liu, Y.C., Lin, Y.C., Kanehara, K., and Nakamura, Y. (2019). A methyltransferase trio essential for phosphatidylcholine biosynthesis and growth. Plant Physiol. **179:** 433–445.

Mansour, M.M.F. (1995). Changes in cell membrane permeability and lipid content of wheat root cortex cells induced by NaCl. Biol. Plant **37:** 143–145.

Markakis, M.N., De Cnodder, T., Lewandowski, M., Simon, D., Boron, A., Balcerowicz, D., Doubbo, T., Taconnat, L., Renou, J.P., Höfte, H., Verbelen, J.P., and Vissenberg, K. (2012). Identification of genes involved in the ACC-mediated control of root cell elongation in *Arabidopsis thaliana*. BMC Plant Biol. **12:** 208.

Mathelier, A., Fornes, O., Arenillas, D.J., Chen, C., Denay, G., Lee, J., Shi, W., Shyr, C., Tan, G., Worsley-Hunt, R., Zhang, A.W., Parcy, F., Lenhard, B., Sandelin, A., and Wasserman, W.W. (2016). JASPAR 2016: A major expansion and update of the open-access database of transcription factor binding profiles. Nucleic Acids Res. **44:** D110–D115.

Matyash, V., Liebisch, G., Kurzchalia, T.V., Shevchenko, A., and Schwudke, D. (2008). Lipid extraction by methyl-tert-butyl ether for high-throughput lipidomics. J. Lipid Res. **49:** 1137–1146.

Mou, Z.L., Wang, X.Q., Fu, Z.M., Dai, Y., Han, C., Ouyang, J., Bao, F., Hu, Y.X., and Li, J.Y. (2002). Silencing of phosphoethanolamine *N*-methyltransferase results in temperature-sensitive male sterility and salt hypersensitivity in *Arabidopsis*. Plant Cell **14:** 2031–2043.

Munns, R., and Tester, M. (2008). Mechanisms of salinity tolerance. Annu. Rev. Plant Biol. **59:** 651–681.

Ngo, A.H., Kanehara, K., and Nakamura, Y. (2019). Non-specific phospholipases C, NPC2 and NPC6, are required for root growth in *Arabidopsis*. Plant J. **100:** 825–835.

Noctor, G., and Foyer, C.H. (1998). Ascorbate and glutathione: keeping active oxygen under control. Annu. Rev. Plant Physiol. Plant Mol. Biol. **49:** 249–279.

Ober, E.S., and Sharp, R.E. (1994). Proline accumulation in maize (*Zea mays* L.) primary roots at low water potentials (i. requirement for increased levels of abscisic acid). Plant Physiol. **105:** 981–987.

Owusu-Ansah, E., and Banerjee, U. (2009). Reactive oxygen species prime *Drosophila* haematopoietic progenitors for differentiation. Nature **461:** 537–541.

Péret, B., Larrieu, A., and Bennett, M.J. (2009). Lateral root emergence: A difficult birth. J. Exp. Bot. **60:** 3637–3643.

Perilli, S., Mambro, R.D., and Sabatini, S. (2012). Growth and development of the root apical meristem. Curr. Opin. Plant Biol. **15:** 17–23.

Salama, K.H.A., Mansour, M.M.F., Ali, F.Z.M., and Abou-hadid, A.F. (2007). NaCl-induced changes in plasma membrane lipids and proteins of *Zea mays* L. cultivars ldiffering in their response to salinity. Acta Physiol. Plant. **29:** 351.

Sartain, M., Salcedo, J., Murali, A., Li, X., Stow, S., and Koelmel, J. (2019). Improving Coverage of The Plasma Lipidome Using Iterative MS/MS Data Acquisition Combined With Lipid Annotator Software And 6546 LC/Q-TOF. Agilent Application Note 2019 5994–0775en.

Saucedo-García, M., Gavilanes-Ruíz, M., and Arce-Cervantes, O. (2015). Long-chain bases, phosphatidic acid, MAPKs, and reactive oxygen species as nodal signal transducers in stress responses in *Arabidopsis*. Front. Plant Sci. **6:** 55.

Sun, J., Li, L., Liu, M., Wang, M., Ding, M., Deng, S., Lu, C., Zhou, X., Shen, X., Zheng, X., and Chen, S. (2010). Hydrogen peroxide and nitric oxide mediate K^+/Na^+ homeostasis and antioxidant defense in NaCl-stressed callus cells of two contrasting poplars. Plant Cell Tiss. Organ Cult. **103:** 205–215.

Sun, L.R., Wang, Y.B., He, S.B., and Hao, F.S. (2018). Mechanisms for abscisic acid inhibition of primary root growth. Plant Signal. Behav. **13:** e1500069.

Tabuchi, T., Okada, T., Azuma, T., Nanmori, T., and Yasuda, T. (2006). Posttranscriptional regulation by the upstream open reading frame of the phosphoethanolamine *N*-methyltransferase gene. Biosci. Biotechnol. Biochem. **70:** 2330–2334.

Vanneste, S., and Friml, J. (2009). Auxin: A trigger for change in plant development. Cell **136:** 1005–1016.

Verslues, P.E., Agarwal, M., Katiyar-Agarwal, S., Zhu, J.H., and Zhu, J.K. (2006). Methods and concepts in quantifying resistance to drought, salt and freezing, abiotic stresses that affect plant water status. Plant J. **45:** 523–539.

Vishwakarma, K., Upadhyay, N., Kumar, N., Yadav, G., Singh, J., Mishra, R.K., Kumar, V., Verma, R., Upadhyay, R.G., Pandey, M., and Sharma, S. (2017). Abscisic acid signaling and abiotic stress tolerance in plants: A review on current knowledge and future prospects. Front. Plant Sci. **8:** 161.

Wang, L., Hua, D.P., He, J.N., Duan, Y., Chen, Z.Z., Hong, X.H., and Gong, Z.Z. (2011). *Auxin Response Factor2 (ARF2)* and its regulated homeodomain gene *HB33* mediate abscisic acid response in *Arabidopsis*. PLoS Genet. **7:** e1002172.

Wang, S., Uddin, M.I., Tanaka, K., Yin, L., Shi, Z., Qi, Y., Mano, J., Matsui, K., Shimomura, N., Sakaki, T., Deng, X., and Zhang, S. (2014). Maintenance of chloroplast structure and function by overexpression of the rice *Monogalactosyldiacylglycerol synthase* gene leads to enhanced salt tolerance in tobacco. Plant Physiol. **165:** 1144–1155.

Xing, H.L., Dong, L., Wang, Z.P., Zhang, H.Y., Han, C.Y., Liu, B., Wang, X.C., and Chen, Q.J. (2014). A CRISPR/Cas9 toolkit for multiplex genome editing in plants. BMC Plant Biol. **14:** 327.

Xu, J.M., Wang, Z.Q., Wang, J.Y., Li, P.F., Jin, J.F., Chen, W.W., Fan, W., Kochian, L.V., Zheng, S.J., and Yang, J.L. (2020). Low phosphate represses histone deacetylase complex1 to regulate root system architecture remodeling in *Arabidopsis*. New Phytol. **225:** 1732–1745.

Yamada, M., Han, X.W., and Benfey, P.N. (2020). RGF1 controls root meristem size through ROS signalling. Nature **577:** 85–88.

Yang, L., Zhang, J., He, J.N., Qin, Y.Y., Hua, D.P., Duan, Y., Chen, Z.Z., and Gong, Z.Z. (2014). ABA-mediated ROS in mitochondria regulate root meristem activity by controlling plethora expression in *Arabidopsis*. PLoS Genet. **10:** e1004791.

Yang, Y.Q., and Guo, Y. (2018). Unraveling salt stress signaling in plants. J. Integr. Plant Biol. **60:** 796–804.

Yang, Z.J., Wang, C.W., Xue, Y., Liu, X., Chen, S., Song, C.P., Yang, Y. Q., and Guo, Y. (2019). Calcium-activated 14-3-3 proteins as a molecular switch in salt stress tolerance. Nat. Commun. **10:** 1199.

Yoshida, T., Christmann, A., Yamaguchi-Shinozaki, K., Grill, E., and Fernie, A.R. (2019). Revisiting the basal role of ABA – Roles outside of stress. Trends Plant Sci. **24:** 625–635.

Yuan, S.R., Li, Z.G., Li, D.Y., Yuan, N., Hu, Q., and Luo, H. (2015). Constitutive expression of rice *microRNA528* alters plant development and enhances tolerance to salinity stress and nitrogen starvation in creeping bentgrass. Plant Physiol. **169:** 576–593.

Zhang, H.M., Han, W., De Smet, I., Talboys, P., Loya, R., Hassan, A., Rong, H.L., Juergens, G., Knox, J.P., and Wang, M.H. (2010). ABA promotes quiescence of the quiescent centre and suppresses stem cell differentiation in the *Arabidopsis* primary root meristem. Plant J. **64:** 764–774.

Zhao, C.Z., Zayed, O., Yu, Z.P., Jiang, W., Zhu, P.P., Hsu, C.C., Zhang, L.R., Tao, W.A., Lozano-Duran, R., and Zhu, J.K. (2018a). Leucine-rich repeat extensin proteins regulate plant salt tolerance in *Arabidopsis*. Proc. Natl. Acad. Sci. U.S.A. **115:** 13123–13128.

Zhao, C.Z., Zhang, H., Song, C.P., Zhu, J.K., and Shabala, S. (2020). Mechanisms of plant responses and adaptation to soil salinity. Innovation **1:** 100017.

Zhao, Y., Zhang, Z.J., Gao, J.H., Wang, P.C., Hu, T., Wang, Z.G., Hou, Y.J., Wan, Y.Z., Liu, W.S., Xie, S.J., Lu, T., Xue, L., Liu, Y., Macho, A. P., Tao, W.A., Bressan, R.A., and Zhu, J.K. (2018b). *Arabidopsis* duodecuple mutant of PYL ABA receptors reveals PYL repression of ABA-independent SnRK2 activity. Cell Rep. **23:** 3340–3351.

Zhou, H.P., Zhao, J.F., Yang, Y.Q., Chen, C.X., Liu, Y.F., Jin, X.H., Chen, L.M., Li, X.Y., Deng, X.W., Schumaker, K.S., and Guo, Y. (2012). Ubiquitin-specific protease16 modulates salt tolerance in *Arabidopsis* by regulating Na^+/H^+ antiport activity and serine hydroxymethyltransferase stability. Plant Cell **24:** 5106–5122.

Zhu, J.K. (2002). Salt and drought stress signal transduction in plants. Annu. Rev. Plant Biol. **53:** 247–273.

Zou, Y., Zhang, X.J., Tan, Y.Y., Huang, J.B., Zheng, Z.Q., and Tao, L.Z. (2019). Phosphoethanolamine *N*-methyltransferase 1 contributes to maintenance of root apical meristem by affecting ROS and auxin-regulated cell differentiation in *Arabidopsis*. New Phytol. **224:** 258–273.

SUPPORTING INFORMATION

Additional Supporting Information may be found online in the supporting information tab for this article: http://onlinelibrary.wiley.com/doi/10.1111/jipb.13326/suppinfo

Figure S1. Accelerated cell differentiation in SALK_108751 after salt stress

Figure S2. SALK_108751 show retarded growth under different salt treatment

Figure S3. FDH is not required for the salt-hypersensitive phenotype

Figure S4. Exogenous ChoCl rescued the salt-hypersensitive phenotype of the SALK_108751

Figure S5. Overexpression lines of *PMT1* identification

Figure S6. PMT1 functions non-redundantly to regulate salt tolerance

Figure S7. Salt phenotypes of phosphoethanolamine *N*-methyltransferase (PMT) loss-of-function mutation

Figure S8. PMT1 regulates root meristem activity under salt stress

Figure S9. Cell membrane integrity and root length in *pmt1* is related to glycerolipid

Figure S10. Relative change of glycolipid in wild-type (WT) and *pmt1-2* after NaCl treatment

Figure S11. The transcription regulation analysis revealed the involvement of abscisic acid (ABA) signaling in *PMT1* expression

Figure S12. Abscisic acid (ABA) content in wild-type (WT) and *pmt1-2* with or without salt treatment

Figure S13. Abscisic acid (ABA) mimics salt stress to affect cell division and auxin response change

Figure S14. Identification of *pmt1-2 aba2-1* homozygous lines

Figure S15. Loss-of-function mutation of *ABA2* in SALK_108751 could recover salt sensitivity of SALK_108751

Table S1. Primer pairs used in this present study